

# Spacetime-Efficient Low-Depth Quantum State Preparation with Applications

Kaiwen Gui,<sup>1,2,3,\*</sup> Alexander M. Dalzell,<sup>4,5,\*</sup> Alessandro Achille,<sup>6</sup> Martin Suchara,<sup>1</sup> and Frederic T. Chong<sup>3</sup>

<sup>1</sup>Amazon Web Services, WA, USA

<sup>2</sup>Pritzker School of Molecular Engineering, University of Chicago, IL, USA

<sup>3</sup>Department of Computer Science, University of Chicago, IL, USA

<sup>4</sup>AWS Center for Quantum Computing, Pasadena, CA, USA

<sup>5</sup>California Institute of Technology, Pasadena, CA, USA

<sup>6</sup>AWS AI Labs, Pasadena, CA, USA

(Dated: March 6, 2023)

We propose a novel deterministic method for preparing arbitrary quantum states, and we show that it requires asymptotically fewer quantum resources than previous methods. When our protocol is compiled into CNOT and arbitrary single-qubit gates, it prepares an  $N$ -dimensional state in depth  $O(\log(N))$  and *spacetime allocation* (a metric that accounts for the fact that oftentimes some ancilla qubits need not be active for the entire protocol)  $O(N)$ , which are both optimal and not simultaneously achieved by previous methods. When compiled into the  $\{\text{H}, \text{S}, \text{T}, \text{CNOT}\}$  gate set, it prepares an arbitrary state up to error  $\epsilon$  in depth  $O(\log(N/\epsilon))$  and spacetime allocation  $O(N \log(\log(N)/\epsilon))$ , improving over  $O(\log(N) \log(N/\epsilon))$  and  $O(N \log(N/\epsilon))$ , respectively. We illustrate how the reduced spacetime allocation of our protocol enables rapid preparation of many disjoint states with only constant-factor ancilla overhead —  $O(N)$  ancilla qubits are reused efficiently to prepare a product state of  $w$   $N$ -dimensional states in depth  $O(w + \log(N))$  rather than  $O(w \log(N))$ , achieving effectively constant depth per state. We highlight several applications where this ability would be useful, including quantum machine learning, Hamiltonian simulation, and solving linear systems of equations. We provide quantum circuit descriptions of our protocol along with detailed pseudocode.

## I. INTRODUCTION

Quantum state preparation (QSP) is a crucial subroutine in many proposed quantum algorithms that claim super-polynomial speedup over their classical counterparts in applications such as quantum machine learning [1–8], simulating quantum systems [9–12], solving linear systems of equations [13–15], and synthesizing unitary operations [16–18].

In a typical state preparation setting, we wish to create a quantum state of the form:

$$|\psi\rangle = \frac{1}{\|\mathbf{x}\|} \sum_{i=0}^{2^n-1} x_i |i\rangle \quad (1)$$

where  $n$  denotes the number of qubits,  $\|\cdot\|$  denotes the standard Euclidean norm, and  $\mathbf{x}$  is a  $2^n$ -dimensional vector with components  $x_i \in \mathbb{C}$ . In many applications, it is sufficient to let  $x_i \in \mathbb{R}^+ \cup \{0\}$ , and henceforth we assume this for simplicity; the additional phase information can be easily incorporated with minimal overhead (see App. B). We also denote  $N = 2^n$  as the total number of parameters encoded, the same as the dimension of the vector space.

Recent advancement by Sun et al. [17] gave an optimal construction that creates  $|\psi\rangle$  with  $\Theta(2^n/n)$ <sup>1</sup> circuit depth

\* These two authors contributed equally;

kgui@uchicago.edu, dalzel@amazon.com

<sup>1</sup> Throughout the paper, we use  $O(f(n, 1/\epsilon))$  notation to indicate that the cost scales as a constant number times  $f(n, 1/\epsilon)$  as  $n, 1/\epsilon \rightarrow \infty$ . We use  $\Theta(f(n, 1/\epsilon))$  when, additionally, the scaling is known to saturate a lower bound, up to constant factors.

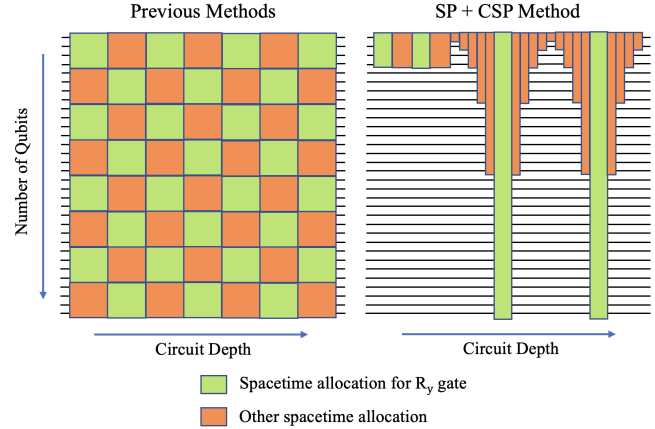


Figure 1: Illustration of spacetime allocation in our state preparation protocol (SP + CSP) versus previous methods. Green regions correspond to spacetime allocated for arbitrary single-qubit rotations. Orange regions correspond to spacetime allocated to qubits that are active (i.e. not in the state  $|0\rangle$ ) but not experiencing arbitrary single-qubit rotations; these qubits might experience CNOT or Toffoli gates, for example, or they might be idling while entangled with other qubits. In our method, the spacetime allocation is asymptotically smaller than the product of qubit count and depth. Additionally, unlike previous methods, our method performs all the single-qubit  $R_y$  rotation gates in parallel during  $O(1)$  separate layers.

without using ancilla qubits, using arbitrary single-qubit gates and two-qubit CNOT gates (henceforth called the  $\{\text{U}(2), \text{CNOT}\}$  gate set). On the other hand, one can

Gate Set	$\{\text{U}(2), \text{CNOT}\}$		$\{\text{H}, \text{S}, \text{T}, \text{CNOT}\}$	
	Depth	Spacetime Allocation	Depth	Spacetime Allocation
Sun et al. [17]	$O(\log(N) \log(\log(N)))$	$\Theta(N)$	$O(\log(N) \log(\log(N)) \log(N/\epsilon))$	$O(N \log(N/\epsilon))$
Sun et al. [17]	$\Theta(\log N)$	$O(N \log N)$	$O(\log(N) \log(N/\epsilon))$	$O(N \log(N) \log(N/\epsilon))$
Zhang et al. [19]	$\Theta(\log N)$	$O(N \log N)$	$O(\log(N) \log(\log(N)/\epsilon))$	$O(N \log(N) \log(\log(N)/\epsilon))$
Clader et al. [20]	$\Theta(\log N)^*$	$O(N \log N)^*$	$O(\log(N/\epsilon))^*$	$O(N \log(N/\epsilon))^*$
<b>This Work (SP)</b>	$\Theta(\log N)$	$O(N \log(N))$	$O(\log(N/\epsilon))$	$O(N \log(N/\epsilon))$
<b>This Work (SP + CSP)</b>	$\Theta(\log N)$	$\Theta(N)$	$O(\log(N/\epsilon))$	$O(N \log(\log(N)/\epsilon))$

Table I: Comparison of our results to previous state-of-the-art low-depth QSP methods. Here,  $N = 2^n$  is the total number of basis/parameters and  $\epsilon$  is the error precision parameter. Note that Sun et al. [17] proposed additional variations of the QSP protocol with larger circuit depth and fewer ancilla qubits that all have spacetime allocation of  $\Theta(N)$  and  $O(N \log(N/\epsilon))$ . The asterisk \* in the row for Ref. [20] indicates that there it was assumed that FANOUT-CNOT could be performed in a single time step.

also use additional ancilla qubits to reduce the circuit depth. It is preferable to use low-depth protocols in situations where one has access to large quantities of ancilla qubits, and when the state-preparation procedure needs to be completed quickly or needs to be repeated many times sequentially. Oftentimes, the quantum algorithm that follows the preparation of  $|\psi\rangle$ —for instance, making a machine learning inference—runs in depth  $\text{poly}(n)$ , exponentially faster than the ancilla-free QSP implementations, so low-depth state preparation is vital to make the overall runtime reasonable.

Toward that end, recent deterministic methods [17, 19] have achieved optimal  $\Theta(n)$  quantum circuit depth in the  $\{\text{U}(2), \text{CNOT}\}$  gate set. However, this exponential depth reduction comes with an exponential overhead in space. In other words, one would need  $O(N)$  many ancilla qubits.

When considering the total required quantum resource tradeoffs, metrics such as circuit depth, circuit size, and qubit count are typically considered. Assuming the physical architecture allows one to perform gates in parallel, the circuit depth is a proxy for the overall runtime of the computation, and the qubit count represents the overall amount of space that must be allocated to the computation. We now propose another metric, **spacetime allocation**—the total time of each individual qubit must be active (i.e., not in the  $|0\rangle$  state). The spacetime allocation is bounded below by the circuit size and bounded above by the product of the qubit count and the circuit depth, but it carries a distinct operational meaning. In a model where one wishes to perform many distinct ancilla-intensive jobs (such as rapidly preparing many independent  $n$ -qubit states) with a fixed number of ancilla qubits, the availability of fresh ancillae in the state  $|0\rangle$  becomes the algorithmic bottleneck. Assuming ancillae can be reallocated from one job to another as soon as they are returned to the  $|0\rangle$  state, the overall running time to complete the batch of jobs is determined by the spacetime allocation of the jobs rather than their depth or size. State-preparation algorithms that are optimal

in terms of depth or size are not necessarily also optimal in terms of spacetime allocation. We will show that, when compiled into the  $\{\text{U}(2), \text{CNOT}\}$  gate set, our state preparation protocol is simultaneously optimal in depth, size, and spacetime allocation, up to constant factors.

In practice, it may not be possible to perform arbitrary single-qubit gates to exact precision. In this case, we cannot hope to prepare the state  $|\psi\rangle$  exactly; rather, given an error parameter  $\epsilon$ , we seek to prepare a state  $|\tilde{\psi}\rangle$  such that

$$\| |\psi\rangle - |\tilde{\psi}\rangle \| \leq \epsilon. \quad (2)$$

For example, this is the case in most proposals for fault-tolerant quantum computation based on error-correcting codes, where logical single qubit gates are approximately performed using a sequence of logical gates drawn from a discrete gate set (see, e.g., [21]). A common choice of discrete gate set is  $\{\text{H}, \text{S}, \text{T}, \text{CNOT}\}$  (defined in the next section); we quote the scaling of the resource cost of our protocol for approximate QSP when compiled into this gate set. We use the terminology **approximate spacetime allocation** and **exact spacetime allocation**, denoted as  $\text{SA}_{\text{approx}}$  and  $\text{SA}_{\text{exact}}$ , to differentiate the cost in the two models. Similarly, we denote the circuit depth in the two models by  $\text{D}_{\text{approx}}$  and  $\text{D}_{\text{exact}}$ .

Another feature of our constructions is that they are garbage free. This contrasts with some previous work (e.g., [22, 23]), which perform a relaxed version of the QSP task, where, instead of preparing the  $n$ -qubit state  $|\psi\rangle$ , one aims to prepare an  $(n+a)$ -qubit state  $|\Psi\rangle$  given by

$$|\Psi\rangle = \frac{1}{\|\mathbf{x}\|} \sum_{i=0}^{2^n-1} x_i |i\rangle \otimes |\text{garbage}_i\rangle. \quad (3)$$

Typically,  $a$  would scale at least linearly in  $n$ ; these  $a$  qubits are left entangled with the  $n$  data qubits. Allowing garbage makes the QSP task easier, and in some applications, garbage is tolerable. However, as long as the

$a$  ancilla qubits are entangled with the data, they cannot be used as fresh  $|0\rangle$  ancillae for other tasks, and they continue to contribute toward the spacetime allocation of the QSP protocol.

The contributions of this work are the following:

1. We propose a novel, deterministic, garbage-free quantum state preparation method, which we call SP + CSP (Section III), and we show that in the  $\{\text{U}(2), \text{CNOT}\}$  gate set it simultaneously achieves optimal depth and spacetime allocation, a feature not shared by any previous low depth method. We also show that in the  $\{\text{H}, \text{S}, \text{T}, \text{CNOT}\}$  gate set, it achieves depth and spacetime allocation that are both asymptotically superior to previous methods (see Table I).
2. We show how the optimal spacetime allocation of our protocol allows it to prepare multiple copies of a state more rapidly than other methods (Section IV).
3. We discuss several applications of the optimal spacetime allocation quantum state preparation protocol (Section V), including
  - (a) Quantum Machine Learning
  - (b) Hamiltonian simulation
  - (c) Solving linear systems with HHL-style quantum algorithms
4. We provide the circuit-level implementation for the SP + CSP method (Section III & Appendix A) with detailed pseudocode.

We summarize our result compared to other state-of-the-art results in Table I, with a pictorial depiction in Fig. 1.

To achieve these results, we build from the work of Clader et al. [20]. The state preparation protocol of Ref. [20] performed all of the single-qubit rotations in  $O(1)$  parallel layers, allowing it to achieve  $\Theta(\log(N/\epsilon))$  depth in the  $\{\text{H}, \text{S}, \text{T}, \text{CNOT}, \text{FANOUT-CNOT}\}$  gate set. The FANOUT-CNOT was necessary to perform many CSWAP gates with a common control in  $O(1)$  depth. We show how one can eliminate the need for FANOUT-CNOT with only constant-factor overhead in the number of ancilla qubits and the depth. The basic idea is to copy the control bit into ancilla bits in logarithmic depth, so that all CSWAP gates can proceed in parallel. However, this observation is not alone sufficient—to achieve  $O(n)$  overall depth we require a method that alternates between copying layers and CSWAP layers (see App. A 3). This constitutes what we call the SP protocol.

The SP protocol does not achieve optimal spacetime allocation, as it fundamentally requires  $O(N)$  ancilla qubits to be entangled with the  $O(n)$  data qubits for a constant fraction of the circuit depth. To circumvent this, we provide a new idea: prepare roughly half of the qubits using

the SP method, and then perform *controlled state preparation* (CSP) from those qubits into the rest of the qubits. Both SP and CSP require only  $O(1)$  layers of single-qubit rotations, preserving the  $O(\log(N/\epsilon))$  depth for the approximate compilation. Moreover, the full  $O(N)$  ancilla qubits are only needed very briefly during the CSP procedure, and most can be freed up after only  $O(1)$  depth. Ultimately, we show that  $O(N)$  spacetime allocation can be achieved.

## II. BACKGROUND

This section will introduce the required quantum gates and provide more details about the spacetime allocation metric as well as relevant lower bounds and a summary of the relevant prior work.

### A. Quantum Gates

In this work, we will use the following quantum gates: X gate, S gate, T gate, Hadamard (H) gate,  $R_y$  gate, CNOT gate, SWAP gate, controlled- $R_y$  gate, Fredkin gate, and Toffoli gate.

Gate	Unitary
X	$\begin{pmatrix} 0 & 1 \\ 1 & 0 \end{pmatrix}$
Hadamard (H)	$\begin{pmatrix} \frac{1}{\sqrt{2}} & \frac{1}{\sqrt{2}} \\ \frac{1}{\sqrt{2}} & -\frac{1}{\sqrt{2}} \end{pmatrix}$
Y-Rotation ( $R_y(\theta)$ )	$\begin{pmatrix} \cos \frac{\theta}{2} & -\sin \frac{\theta}{2} \\ \sin \frac{\theta}{2} & \cos \frac{\theta}{2} \end{pmatrix}$
CNOT	$\begin{pmatrix} 1 & 0 & 0 & 0 \\ 0 & 1 & 0 & 0 \\ 0 & 0 & 0 & 1 \\ 0 & 0 & 1 & 0 \end{pmatrix}$
S	$\begin{pmatrix} 1 & 0 \\ 0 & i \end{pmatrix}$
T	$\begin{pmatrix} 1 & 0 \\ 0 & e^{\frac{i\pi}{4}} \end{pmatrix}$

Table II: Elementary Quantum Gates. Note that there is some redundancy as  $S = T^2$  and  $X = HS^2H$ . The  $R_y$  gate can be approximated to arbitrary precision as a sequence of H, S, and T gates (see, e.g., [21])

Table II shows the elementary quantum gates required for the  $\{\text{U}(2), \text{CNOT}\}$  gate set and the  $\{\text{H}, \text{S}, \text{T}, \text{CNOT}\}$  gate set. We also summarize all other required quantum gates that can be constructed in Fig. 2, 3, 4, and 5.

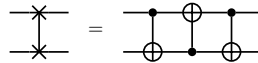


Figure 2: SWAP Gate Decomposition Using CNOT

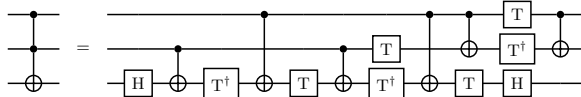


Figure 3: Toffoli (CCNOT) Gate Decomposition Using H, T, CNOT [24]

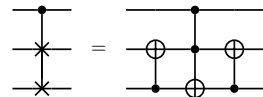


Figure 4: Fredkin (CSWAP) Gate Decomposition Using CNOT, Toffoli [25]

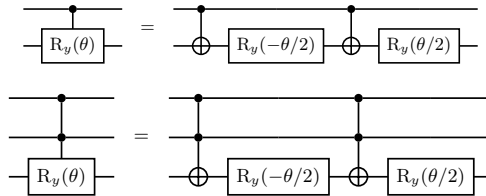


Figure 5: Controlled Rotation Gate Decomposition Using  $R_y$ , CNOT, Toffoli

## B. Spacetime Allocation - QPU “Core Hours”

In classical computing, “core hours” refers to the number of CPUs used to run a certain computing task multiplied by the duration of the job in hours. We now define the quantum analogy of the classical “core hours” as the quantum spacetime allocation cost which is equivalently defined in either of the following ways

- Sum of the individual duration (depth) that each logical qubit is active (i.e., not in the  $|0\rangle$  state)
- Sum of the number of active qubits in each layer

Or quantitatively:

$$SA := \sum_{i=0}^{q-1} d_i = \sum_{t=0}^{d-1} q_t \quad (4)$$

where  $d$  is the total depth,  $q$  is the total number of qubits,  $d_i$  is the active time (depth) for the  $i$ th qubit, and  $q_t$  is the number of active qubits at layer  $t$ .

In the case that all qubits are active for the entirety of the computation, the spacetime allocation is simply

the product of the circuit depth and the total number of qubits. However, if most of the ancilla qubits are needed only briefly and can be reset to the  $|0\rangle$  state before the end of the computation, the spacetime allocation can be significantly less [26]. In this work, we will show that freeing up the ancilla qubits at early times can bring asymptotic spacetime allocation advantage for quantum state preparation.

## C. Lower Bounds

Previous work has shown QSP lower bounds for circuit depth, size, number of qubits and tradeoffs therein [17, 27] when using only arbitrary single-qubit gates and CNOT gates. Since each gate in the circuit acts on at least one qubit, at least one qubit must be active per gate in each layer. Thus, the number of gates provides a lower bound for the spacetime allocation.

**Lemma II.1.** *If a quantum circuit has circuit size  $C$ , its spacetime allocation must be at least  $C$ .*

Thus, if we wish to lower bound the spacetime allocation, it suffices to bound the circuit size. An arbitrary quantum state is described by  $O(2^n)$  real parameters. Each single-qubit gate can introduce at most  $O(1)$  real parameters, so there must be  $O(2^n)$  single-qubit gates. Additionally, any consecutive single-qubit gates on the same qubit that do not have a CNOT in between can be combined into a single gate, so the number of CNOTs must be on the same order as the number of single-qubit gates. This line of reasoning gives rise to a lower bound on circuit size [27].

**Lemma II.2** (Section II of [27]). *A quantum circuit consisting of gates drawn from  $\{U(2), \text{CNOT}\}$  that prepares an arbitrary  $n$ -qubit quantum state must have at least  $\Omega(2^n)$  CNOT gates and at least  $\Omega(2^n)$   $U(2)$  gates.*

**Corollary II.2.1.** *A quantum circuit consisting of gates drawn from  $\{U(2), \text{CNOT}\}$  that prepares an arbitrary  $n$ -qubit quantum state must have at least  $\Omega(2^n)$  spacetime allocation.*

Similar lower bounds are possible in the  $\{H, S, T, \text{CNOT}\}$  gate set by counting arguments.

**Theorem II.3.** (Eq. (4.85) of [28]) *A quantum circuit consisting of gates drawn from  $\{H, S, T, \text{CNOT}\}$  that prepares an arbitrary  $n$ -qubit state to error  $\epsilon$  must have at least  $\Omega\left(\frac{2^n \log(1/\epsilon)}{\log n}\right)$  gates.*

Note that Ref. [16] has shown that the number of T gates can be significantly smaller than this lower bound, an interesting fact since T gates are significantly more expensive than the other gates in many approaches to fault-tolerant quantum computation.

**Corollary II.3.1.** *A quantum circuit consisting of gates drawn from  $\{H, S, T, \text{CNOT}\}$  for preparing an arbitrary*

$n$ -qubit state to error  $\epsilon$  must have at least  $\Omega\left(\frac{2^n \log(1/\epsilon)}{\log n}\right)$  spacetime allocation.

Future work might aim to determine if the lower bound in Corollary II.3.1 is tight.

## D. Upper Bounds in Prior Work

### 1. $\{\text{U}(2), \text{CNOT}\}$ gate set

To the best of our knowledge, the state-of-the-art quantum state preparation [17, 19, 20] methods achieve the following depth (depending on the number of ancillae):

$$D_{\text{exact}} = \begin{cases} \Theta\left(\frac{2^n}{n}\right), & \text{if } a = 0 \text{ (need } n \text{ data qubits)} \\ \Theta(n \log n), & \text{if } a = O\left(\frac{2^n}{n \log n}\right) \\ \Theta(n), & \text{if } a = O(2^n) \end{cases}$$

Here  $D_{\text{exact}}$  labels the depth of the exact quantum state preparation circuit using the  $\{\text{U}(2), \text{CNOT}\}$  gate set,  $a$  denotes the number of ancillae, and  $n$  denotes the number of qubits of the desired arbitrary quantum state to be prepared.

We can compute the spacetime allocation upper bound by simply multiplying the depth with the number of qubits required for these results, as it does not appear that a sufficient number of ancilla qubits are freed up sufficiently early to make an asymptotic difference:

$$SA_{\text{exact}} = \begin{cases} \Theta(2^n), & \text{if } D_{\text{exact}} = \Theta\left(\frac{2^n}{n}\right) \\ \Theta(2^n), & \text{if } D_{\text{exact}} = \Theta(n \log n) \\ O(n2^n), & \text{if } D_{\text{exact}} = \Theta(n) \end{cases}$$

We can see that for circuit depths  $D_{\text{exact}} > \Omega(n \log n)$  the  $\Theta(2^n)$  lower bound for spacetime allocation shown in Corollary II.2.1 is already known to be saturated. Interestingly, Sun et al. [17] has also proved a depth lower bound of  $\Omega(n)$  for circuits that use arbitrary single-qubit and two-qubit gates, regardless of the number of ancillary qubits from a graph theory perspective. Previous methods [17, 19, 20] all have a spacetime allocation upper bound of  $SA_{\text{exact}} = O(n2^n)$  for  $O(n)$  depth. Now the natural question arises: can we find a quantum circuit that simultaneously achieves  $SA_{\text{exact}} = \Theta(2^n)$  and  $D_{\text{exact}} = \Theta(n)$ ? In Sec. III, we show that our SP+CSP state preparation protocol provides a positive answer to this question.

### 2. $\{\text{H}, \text{S}, \text{T}, \text{CNOT}\}$ gate set

When compiled into gates from  $\{\text{H}, \text{S}, \text{T}, \text{CNOT}\}$  previous methods have achieved [17, 19] the following depth:

$$D_{\text{approx}} = \begin{cases} O\left(\frac{2^n \log(2^n/\epsilon)}{n}\right), & \text{if } a = 0 \\ O(n \log(n) \log(2^n/\epsilon)), & \text{if } a = O\left(\frac{2^n}{n \log n}\right) \\ O(n \log(n/\epsilon)), & \text{if } a = O(2^n) \end{cases}$$

We can also compute the spacetime allocation cost by multiplying the circuit depth by the number of qubits involved:

$$SA_{\text{approx}} = \begin{cases} O(2^n \log(2^n/\epsilon)), & \text{if } a = 0 \\ O(2^n \log(2^n/\epsilon)), & \text{if } a = O\left(\frac{2^n}{n \log n}\right) \\ O(2^n n \log(n/\epsilon)), & \text{if } a = O(2^n) \end{cases}$$

Clader et al. [20] gave a method with depth  $O(\log(2^n/\epsilon))$  and spacetime allocation  $O(2^n \log(2^n/\epsilon))$ , but under the assumption of unit time FANOUT-CNOT.

In this work, we will show that our method achieves the depth scaling of Ref. [20] in the  $\{\text{H}, \text{S}, \text{T}, \text{CNOT}\}$  gate set (i.e. not requiring FANOUT-CNOT) while achieving superior spacetime allocation of  $O(2^n \log(n/\epsilon))$ .

## III. SP + CSP STATE PREPARATION

This section will walk through the details of our SP + CSP method that achieves  $\Theta(N)$  spacetime allocation while keeping the  $\Theta(\log N)$  depth using the  $\{\text{U}(2), \text{CNOT}\}$  gate set.

Recall that we wish to create the  $n$ -qubit state  $|\psi\rangle$  in Eq. (1), which has known coefficients  $x_i/\|\mathbf{x}\|$  in the computational basis. We propose to use the following method that uses a combination of a *state preparation* step (SP) on a subset of the data qubits, followed by a *controlled-state preparation* step (CSP). The rationale for doing this rather than a direct state preparation is that the SP + CSP protocol can achieve optimal spacetime allocation scaling even if the underlying SP step does not. The general idea is to partition the  $N = 2^n$  basis states into  $M = 2^m$  non-overlapping sets of size  $\frac{N}{M}$ . Computational basis states for which the first  $m$  bits agree (when written in binary) are placed into the same set. Denote the  $M$  sets by  $J_i$  with  $i = 0, \dots, M-1$ . For each  $i$ , we let  $y_i = \sqrt{\sum_{j \in J_i} |x_j|^2}$ .

We first prepare the state of  $m$  qubits ( $m < n$ ):

$$U_{\text{SP}} |0^m\rangle = |\phi\rangle = \frac{1}{\|\mathbf{y}\|} \sum_{i=0}^{2^m-1} y_i |i\rangle \quad (5)$$

The total state is now  $|\phi\rangle \otimes |0^{n-m}\rangle$ .

Next, we perform the controlled-state preparation operation  $U_{\text{CSP}}$ , defined by

$$U_{\text{CSP}}(|i\rangle \otimes |0^{n-m}\rangle) = y_i^{-1} \sum_{j \in J_i} x_j |j\rangle \quad (6)$$

so that

$$U_{\text{CSP}}(|\phi\rangle \otimes |0^{n-m}\rangle) = |\psi\rangle = \frac{1}{\|\mathbf{x}\|} \sum_{j=0}^{2^n-1} x_j |j\rangle \quad (7)$$

The circuit diagram is shown in Fig. 6.

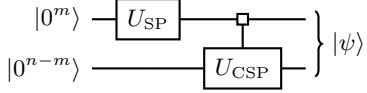


Figure 6: Circuit for SP + CSP procedure that implements state preparation of an arbitrary  $n$ -qubit state  $|\psi\rangle$  by first creating an  $m$ -qubit state  $|\phi\rangle$  and then performing controlled state preparation into the final  $n - m$  qubits. Implementation details of  $U_{\text{SP}}$  and  $U_{\text{CSP}}$  are shown in Fig. 7 and Fig. 8, and involve ancilla qubits not shown in this figure. The square control  $\square$  indicates a different operation is performed on the final  $n - m$  qubits for each of setting of the first  $m$  qubits.

We will now describe how to perform the  $U_{\text{SP}}$  and  $U_{\text{CSP}}$  circuits.

### A. SP Circuit Structure

To perform  $U_{\text{SP}}$ , we give a method that has depth  $O(m)$  and uses  $O(2^m)$  ancilla qubits. The spacetime allocation is thus at most  $O(m2^m)$ . If we require a discrete gate set and have approximation error  $\epsilon$ , this method achieves  $O(m + \log(1/\epsilon))$  depth and spacetime allocation  $O(m2^m + 2^m \log(m/\epsilon))$ .

The idea follows previous literature and begins by defining  $M - 1$  angles that can each be efficiently computed classically from the list of amplitudes  $\{y_i\}_{i=0}^{M-1}$ . For convenience and consistency with previous literature [8], we use a 2-index angle definition to define the rotation angles:

$$\theta_{s,p} = 2 \cos^{-1} \left( \frac{\sqrt{\sum_{l=0}^{2^{m-s-1}-1} |y_{p \cdot 2^{m-s} + l}|^2}}{\sqrt{\sum_{l=0}^{2^{m-s}-1} |y_{p \cdot 2^{m-s} + l}|^2}} \right), \quad (8)$$

where  $s = 0, \dots, m - 1$ , and  $p = 0, \dots, 2^s - 1$ , for a total of  $1 + 2 + 4 + \dots + 2^{m-1} = M - 1$  angles.

This 2-index angle definition will also give us more convenience when labeling the ancilla registers holding the computed angles showed in Eq. 9 and the corresponding data qubits. In particular,  $s$  corresponds to the index of the ancilla register  $A_s$  (referenced in, e.g., algorithm 5) as well as the index of the data qubit being processed. Meanwhile,  $p$  corresponds to the index of the qubit within the particular ancilla register  $A_s$ .

Clader et al. [20] proposed a low-depth strategy for implementing  $U_{\text{SP}}$  using  $O(M)$  ancilla qubits. The general idea is to “pre-rotate” many angles by preparing the

states

$$|\theta_{s,p}\rangle = R_y(\theta_{s,p})|0\rangle = \cos\left(\frac{\theta_{s,p}}{2}\right)|0\rangle + \sin\left(\frac{\theta_{s,p}}{2}\right)|1\rangle \quad (9)$$

in parallel for each  $s = 0, \dots, m - 1$ ,  $p = 0, \dots, 2^s - 1$ , and then efficiently inject a subset of these states into the data qubits. Which states are injected is controlled by the data qubits themselves, leaving the data qubits entangled with a large garbage register. Ref. [20] showed how to uncompute the garbage using a flag mechanism. It was shown that the overall T depth of the computation was  $O(m)$ , but the Clifford depth was not studied, and a naive calculation would suggest the Clifford depth is at least  $O(m^2)$  when we insist on using only two-qubit Clifford gates. Here, we use an adapted version of Ref. [20] by utilizing a bit copying mechanism to guarantee that the Clifford depth is also  $O(m)$ .

The high-level circuit that accomplishes the  $U_{\text{SP}}$  routine is shown in Fig. 7. The circuit describes the gate sequence that prepares an arbitrary  $m$ -qubit state  $|\phi\rangle$  with the assistance of  $2M - 2 = 2^{m+1} - 2$  ancilla qubits that begin and end in  $|0\rangle$ . Note that implementations of the SPF gate and FLAG gate, discussed in App. A, require an additional  $O(M)$  ancillae not shown in the figure to implement the bit copying mechanism mentioned above.

We now follow Ref. [20] and define the action of gates SPF and FLAG that appear in Fig. 7. First, define the product states

$$|\Theta_s\rangle = \bigotimes_{p=0}^{2^s-1} |\theta_{s,p}\rangle \quad \text{for } s = 0, 1, \dots, m - 1$$

$$|\Theta\rangle = \bigotimes_{s=0}^{m-1} |\Theta_s\rangle. \quad (10)$$

Next, for each  $j = 0, \dots, M - 1$ ,  $s = 0, \dots, m - 1$ ,  $p = 0, \dots, 2^s - 1$ , let  $f_{(s,p)|j} = 1$  if the least significant  $s$  digits of the binary representation of  $j$  are equal to  $p$ , and let  $f_{(s,p)|j} = 0$  otherwise. Thus, for each  $j$  and each  $s$ , there is exactly one  $p \in [0, 2^s - 1]$  for which  $f_{(s,p)|j} = 1$ . The values of  $(s, p)$  for which  $f_{(s,p)|j} = 1$  correspond to the angle states  $|\theta_{s,p}\rangle$  that are injected into the data by the SPF circuit for the data qubit setting  $|j\rangle$ .

The  $U_{\text{SP}}$  procedure begins by preparing  $|\Theta\rangle$  into an ancilla “angle” register (register  $A$  in Fig. 7) of size  $M - 1$  using  $M - 1$  parallel  $R_y$  gates. The SPF gate is then applied, which injects some of the angle states into the data and produces the action

$$\text{SPF}(|0^m\rangle |\Theta\rangle) = \frac{1}{\|\mathbf{x}\|} \sum_{j=0}^{M-1} y_j |j\rangle |g_j\rangle. \quad (11)$$

where

$$|g_j\rangle = \bigotimes_{s=0}^{m-1} \bigotimes_{p=0}^{2^s-1} |\theta_{s,p}(1 - f_{(s,p)|j})\rangle. \quad (12)$$

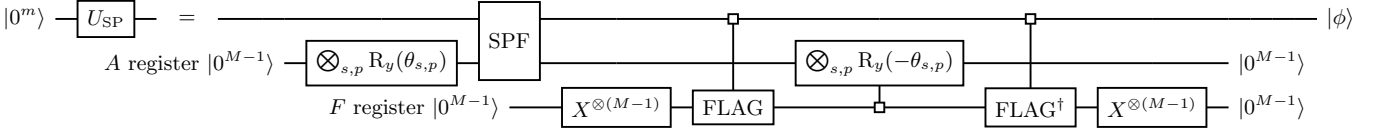


Figure 7: Circuit that implements  $U_{SP}$ , which prepares an arbitrary  $m$ -qubit state from the state  $|0^m\rangle$  with the assistance of  $O(2^m)$  ancillae that begin and end in  $|0\rangle$ . We let  $M = 2^m$  and clarify that the controlled-rotation gate denotes  $M - 1$  controlled-rotations occurring in parallel, by different angles  $\theta_{s,p}$  with  $s = 0, \dots, m - 1$  and  $p = 0, \dots, 2^s - 1$ . Note that the implementation of SPF and FLAG, given in the appendix, involves  $O(M)$  additional unshown ancilla qubits.

Here, the notation  $|\theta(1 - f)\rangle$  is used to denote that the state is  $|\theta\rangle$  when  $f = 0$  and  $|0\rangle$  when  $f = 1$ . In other words, the registers holding  $|\theta_{s,p}\rangle$  for which  $f_{(s,p)|j} = 1$  are replaced with  $|0\rangle$ . We see that the output of SPF has the correct amplitudes as the target state  $|\phi\rangle$ , but leaves the data entangled with an  $(M - 1)$ -qubit garbage register.

The FLAG operation computes the bit  $f_{(s,p)|j}$  into a fresh ancilla “flag” register (register  $F$  in Fig. 7) for each pair  $(s, p)$ , i.e.,

$$\text{FLAG}(|j\rangle |1^{M-1}\rangle) = |j\rangle \bigotimes_{s=0}^{m-1} \bigotimes_{p=0}^{2^s-1} |1 - f_{(s,p)|j}\rangle \quad (13)$$

Thus, by applying a controlled- $R_y(-\theta_{s,p})$  gate controlled by the flag bit  $(1 - f_{(s,p)|j})$  onto the angle qubit in the state  $|\theta_{s,p}(1 - f_{(s,p)|j})\rangle$ , we reset all of the angle qubits back to  $|0\rangle$ . This is done in parallel for each pair  $(s, p)$ . Finally, the adjoint of the FLAG gate can be applied to uncompute the flag bits and bring the flag register back to  $|0^{M-1}\rangle$ . The output of this process is the state  $|\phi\rangle$  without any garbage. The construction for SPF and FLAG described in Ref. [20] was only optimized for the T-depth and T-count. The Clifford count and depth were not explicitly studied. Moreover, it was assumed that a FANOUT-CNOT gate with an arbitrary number of targets could be performed in a single time step.

We document the pseudocode of the SP circuit implementation in algorithm 1.

---

#### Algorithm 1 SP Circuit

---

```

1: procedure SP(data_array,  $m$ ,  $D$ ,  $A$ ,  $F$ )
   ▷  $D$ : data register of size  $m$ 
   ▷  $A$ : angle register of size  $M - 1$ 
   ▷  $F$ : flag register of size  $M - 1$ 
2:   for  $s$  in range( $m$ ) and  $p$  in range( $2^s$ ) do
3:     Classically compute  $\theta_{s,p}$  from  $y$       ▷ Use Eq. (8)
4:   end for
5:   for  $s$  in range( $m$ ) and  $p$  in range( $2^s$ ) do      ▷  $O(1)$ 
6:      $R_y(\theta_{s,p}, A_{s,p})$  onto fresh “angle” ancilla
7:   end for
8:   SPF( $D, A, m$ ) subroutine                  ▷  $O(m)$ 
9:   for  $s$  in range( $m$ ) and  $p$  in range( $2^s$ ) do      ▷  $O(1)$ 
10:     $X(F_{s,p})$  onto fresh “flag” ancilla
11:   end for
12:   FLAG( $D, F, m$ ) subroutine                  ▷  $O(m)$ 
13:   for  $s$  in range( $m$ ) and  $p$  in range( $2^s$ ) do      ▷  $O(1)$ 
14:      $R_y(-\theta_{s,p}, F_{s,p}, A_{s,p})$ 
15:   end for
16:   FLAG $^\dagger$ ( $D, F, m$ ) subroutine            ▷  $O(m)$ 
17:   for  $s$  in range( $m$ ) and  $p$  in range( $2^s$ ) do      ▷  $O(1)$ 
18:      $X(F_{s,p})$  to reset “flag” ancilla to  $|0\rangle$ 
19:   end for
20: end procedure
   ▷ Total Dexact:  $O(m)$ 
   ▷ Total Dapprox:  $O(m + \log(m/\epsilon))$ 
   ▷ Total SAexact:  $O(m2^m)$ 
   ▷ Total SAapprox:  $O(m2^m + 2^m \log(m/\epsilon))$ 

```

---

In the appendix, we detail our constructions for the SPF (Sec. A 3) and FLAG (Sec. A 4) subroutines. There, we illustrate how both subroutines can be performed in  $O(m)$  depth and  $O(m2^m)$  spacetime allocation for both the  $\{U(2), \text{CNOT}\}$  and  $\{\text{H}, \text{S}, \text{T}, \text{CNOT}\}$  gate set.

## B. CSP Circuit Structure

The controlled-state preparation circuit prepares a different  $n - m$  qubit state for each of  $M$  possible settings  $|k\rangle \in \{|0\rangle, \dots, |M-1\rangle\}$  of an  $m$ -qubit control register. Thus, for each  $k$ , there are  $2^{n-m} - 1 = \frac{N}{M} - 1$  angles, which we denote by  $\theta_{s,p}^{(k)}$ , for  $s = 0, \dots, n - m - 1$  and  $p = 0, \dots, 2^s - 1$ . These angles can be computed from

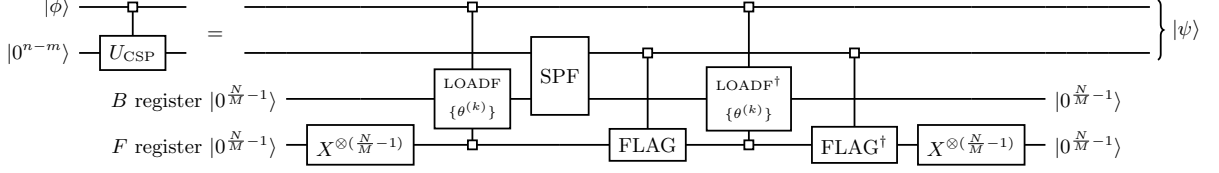


Figure 8: Circuit that implements the  $U_{\text{CSP}}$  operation, which prepares an arbitrary  $n - m$  qubit state for each setting of an  $m$ -qubit control register, with the assistance of  $O(2^{n-m})$  ancillas that begin and end in  $|0\rangle$ . We let  $M = 2^m$  and  $N = 2^n$ . Note that implementation of LOADF, SPF, and FLAG, given in the appendix, involve  $O(N)$  additional unshown ancillae.

the amplitudes of  $\mathbf{x}$  by the equation (c.f. Eq. (8))

$$\theta_{s,p}^{(k)} = 2 \cos^{-1} \left( \frac{\sqrt{\sum_{l=0}^{2^{n-m-s-1}-1} |x_{k2^{n-m}+p \cdot 2^{n-m-s}+l}|^2}}{\sqrt{\sum_{l=0}^{2^{n-m-s}-1} |x_{k2^{n-m}+p \cdot 2^{n-m-s}+l}|^2}} \right). \quad (14)$$

The total number of angles is  $N - M$ . The states  $|\theta_{s,p}^{(k)}\rangle$  are then defined as in Eq. (9), and the product states  $|\Theta_s^{(k)}\rangle$  and  $|\Theta^{(k)}\rangle$  as in Eq. (10). We document the pseudocode of the CSP circuit implementation in algorithm 2.

---

### Algorithm 2 CSP Circuit

---

```

1: procedure CSP(data_array,  $m$ ,  $n$ ,  $D$ ,  $B$ ,  $F$ )
   ▷  $D$ : data register of size  $m - n$ 
   ▷  $B$ : buffer register of size  $\frac{N}{M} - 1$ 
   ▷  $F$ : flag register of size  $\frac{N}{M} - 1$ 
2:   for  $k$  in range( $2^m$ ) do
3:     for  $s$  in range( $n - m$ ) and  $p$  in range( $2^s$ ) do
4:       Classically compute  $\theta_{s,p}^{(k)}$  from  $\mathbf{x}$  ▷ Use Eq. (14)
5:       end for
6:   end for
7:   for  $s$  in range( $n - m$ ) and  $p$  in range( $2^s$ ) do ▷  $O(1)$ 
8:      $X(F_{s,p})$  onto fresh “flag” ancilla
9:   end for
10:  LOADF( $D, B, F$ ) $[\theta_{s,p}^{(k)}]$  load angles into buffer ancilla
    ▷  $O(n)$ 
11:  SPF( $D, B, n - m$ ) to prepare  $n - m$  qubit state with
    garbage ▷  $O(n - m)$ 
12:  FLAG( $D, F, n - m$ ) ▷  $O(n - m)$ 
13:  LOADF $^\dagger$ ( $D, B, F$ ) $[\theta_{s,p}^{(k)}]$  to unload angles ▷  $O(n)$ 
14:  FLAG $^\dagger$ ( $D, F, n - m$ ) ▷  $O(n - m)$ 
15:  for  $s$  in range( $n - m$ ) and  $p$  in range( $2^s$ ) do ▷  $O(1)$ 
16:     $X(F_{s,p})$  to reset “flag” ancilla
17:  end for
18: end procedure
   ▷ Total  $D_{\text{exact}}$ :  $O(n)$ 
   ▷ Total  $D_{\text{approx}}$ :  $O(n + \log(n/\epsilon))$ 
   ▷ Total  $SA_{\text{exact}}$ :  $O(2^n)$ 
   ▷ Total  $SA_{\text{approx}}$ :  $O((n - m)2^{n-m} + 2^n \log(n/\epsilon))$ 

```

---

The controlled-state preparation circuit here is a generalized version of the controlled-state preparation circuit proposed in Clader et al. [20], shown in Fig. 8. The general idea of the CSP circuit is to first, controlled on the control register being  $|k\rangle$ , load in the correct state  $|\Theta^{(k)}\rangle$ .

Once this has been done, the same SPF gate as was used for  $U_{\text{SP}}$  protocol injects the correct angles into the  $n - m$  data qubits. A FLAG mechanism similar to that of the  $U_{\text{SP}}$  protocol is then employed to disentangle the data from the angle register and reset the angle register to  $|0^{M-1}\rangle$ .

The loading and unloading is accomplished with a gate we call LOADF, similar to that in Ref. [20], which is defined by the action

$$\begin{aligned} & \text{LOADF} \left( |k\rangle |0^{N/M-1}\rangle \left[ \bigotimes_{s=0}^{m-n-1} \bigotimes_{p=0}^{2^s-1} |f_{s,p}\rangle \right] \right) \\ &= |k\rangle \left[ \bigotimes_{s=0}^{m-n-1} \bigotimes_{p=0}^{2^s-1} |f_{s,p}\theta_{s,p}^{(k)}\rangle \right] \left[ \bigotimes_{s=0}^{m-n-1} \bigotimes_{p=0}^{2^s-1} |f_{s,p}\rangle \right] \end{aligned} \quad (15)$$

Note that if all the flag bits  $f_{s,p}$  are set to 1, the state  $|\Theta^{(k)}\rangle$  is prepared into the second register. Our implementation of LOADF is shown in Fig. 20 in the appendix, and involves an additional  $O(2^n)$  ancilla qubits.

### C. Overall depth and spacetime allocation

In this section, we compute the overall depth and ancilla allocation of our protocol. To verify the stated complexities of subroutines, we refer the reader to the sections where those subroutines are implemented. We state complexities in the  $\{U(2), \text{CNOT}\}$  gate set, and then quote the associated complexity in the  $\{\text{H}, \text{S}, \text{T}, \text{CNOT}\}$  gate set in *parentheses* when it is different. Note that to achieve overall error  $\epsilon$  in state preparation or controlled-state preparation, it suffices to prepare each angle state  $|\theta_{s,p}\rangle$  to precision  $\epsilon/n$ . To see this, note that the protocol is equivalent to a sequence of  $n$  multi-controlled rotations on the data qubits. If every angle is accurate up to error  $\epsilon/n$ , each of these  $n$  unitaries is enacted up to spectral norm error  $\epsilon/n$ , yielding total error at most  $\epsilon$ . A more thorough justification of this appears in Ref. [20].

We begin with  $U_{\text{SP}}$ , implemented as in Fig. 7. The parallel rotation gates and parallel controlled rotation gates are accomplished in depth  $O(1)$  (depth  $O(\log(m/\epsilon))$ ), while the SPF and FLAG gates have depth  $O(m)$ , yielding a total depth  $O(m)$  (total depth  $O(m + \log(1/\epsilon))$ ) =

$O(\log(2^m/\epsilon))$ ). The required total qubits are the  $m + 2M - 2$  that appear in Fig. 7, plus an additional  $O(M)$  needed to perform the SPF and FLAG operations. The product of space and depth gives an immediate upper bound of spacetime allocation  $O(m2^m)$  (spacetime allocation  $O(2^m \log(2^m/\epsilon))$ ), and indeed for  $U_{\text{SP}}$  there is a matching lower bound (up to constant factor).

We now consider  $U_{\text{CSP}}$ . Here, we again note that to perform the operation to  $\epsilon$  precision, it suffices to perform each single-qubit rotation gate to error  $\epsilon/n$ . The LOADF operation has depth  $O(n)$  (depth  $O(n + \log(1/\epsilon))$ ). Meanwhile, in this context, the SPF and FLAG operations each have depth  $O(n-m)$ , yielding total depth  $O(n)$  (total depth  $O(n + \log(1/\epsilon))$ ). The required total qubits are the  $n + 2N/M$  that appear in Fig. 8, plus the additional  $O(N)$  needed to perform the LOADF, SPF, and FLAG gates. The product of space and depth gives an immediate upper bound of spacetime allocation  $O(n2^n)$  (spacetime allocation  $O(2^n \log(2^n/\epsilon))$ ). However, in this case, the actual spacetime allocation is better than the upper bound. The LOADF subroutine achieves spacetime allocation  $O(2^n)$  (spacetime allocation  $O(2^n \log(n/\epsilon))$ ) even though it acts on  $O(2^n)$  qubits depth  $O(n)$  (depth  $O(n + \log(1/\epsilon))$ ). Meanwhile, FLAG and SPF have spacetime allocation  $O(n2^{n-m})$ . In total, the procedure has spacetime allocation  $O(2^n + n2^{n-m})$  (spacetime allocation  $O(2^n \log(n/\epsilon) + n2^{n-m})$ ).

Adding both parts together, the SP+CSP protocol achieves depth  $O(n)$  (depth  $O(n + \log(1/\epsilon))$ ) and has spacetime allocation  $O(2^n + n(2^m + 2^{n-m}))$  (spacetime allocation  $O(2^n \log(n/\epsilon) + n(2^m + 2^{n-m}))$ ). If  $m$  is chosen between  $\lfloor \log n \rfloor$  and  $\lceil n - \log n \rceil$ , we see that the stated result of spacetime allocation  $O(2^n)$  (spacetime allocation  $O(2^n \log(n/\epsilon))$ ) is true.

In retrospect, we can pinpoint the rationale for pursuing the SP+CSP approach to state preparation. The issue with simply performing the  $U_{\text{SP}}$  protocol with  $n = m$  is that it would require  $2^n - 1$  ancilla qubits to store the  $2^n - 1$  angles, and each of these ancillae must remain allocated for the entire  $O(n)$  depth of the circuit. The SP+CSP protocol gets around this by first preparing the  $m$ -qubit state  $|\phi\rangle$ , requiring only  $2^m - 1$  angles, and for each of the  $2^m$  basis states, preparing a different  $n - m$  qubit state in the remaining qubits. The latter operation requires  $2^{n-m} - 1$  angles (stored in the buffer ancilla register B), so we avoid the need for  $O(2^n)$  angle states to be allocated for the entire  $O(n)$  depth. The trick comes from the ability to load the correct set of  $2^{n-m} - 1$  angles among all  $2^n - 2^m$  angles with only  $O(2^n)$  spacetime allocation, which is accomplished by our LOADF implementation presented in the appendix.

#### IV. PREPARING MANY COPIES OF INDEPENDENT QUANTUM STATES

This section will show how we manage to utilize the novel encoding method we proposed in Sec. III to more

efficiently prepare many copies of arbitrary quantum states (same or different ones) using the  $\{\text{U}(2), \text{CNOT}\}$  gate set. Specifically, we consider the task of preparing a product state of  $w$  separate  $N$ -dimensional states as quickly as possible. If we had  $O(wN)$  ancilla qubits, we could perform state preparation on each of the  $w$  copies in parallel for total depth  $O(\log(N))$ . However, in applications,  $N$  is likely to be large, and we may not have so many ancillae. Suppose we have only  $O(N)$  ancilla qubits—enough to prepare one state in  $O(\log(N))$  depth—but not  $O(wN)$ . Naively, we could prepare the  $w$  states in series, incurring depth  $O(w \log(N))$ . However, since the spacetime allocation required for a single state preparation is  $O(N)$ , the spacetime allocation for preparing  $w$  states is  $O(wN)$ , suggesting that if the  $O(N)$  ancillae are used reused optimally, we might achieve  $O(w)$  total depth, rather than  $O(w \log(N))$ . Indeed, we now illustrate that using our SP + CSP protocol one can accomplish the task in depth  $O(w + \log(N))$ , which is constant  $O(1)$  depth per copy when  $w > \Omega(\log(N))$ .

There are two essential properties in the single-copy arbitrary state preparation method we described in section III:

1. all ancilla qubits are disentangled from the data qubits and returned to the  $|0\rangle$  state. The previously used ancillae are ready to act as either new data qubits or new ancilla qubits.
2. the amount of spacetime occupied by active ancilla qubits is only  $O(N)$ , even though the depth is  $O(\log(N))$  and there are  $O(N)$  ancilla qubits.

Thus, once the ancillae are returned to  $|0\rangle$ , they can begin to assist with the next state preparation, even if the previous state preparation has not been completed. We can concatenate and stack many of the state preparation circuits one after another.

Quantitatively speaking, we can prepare many unentangled copies of the same quantum state

$$|\psi\rangle^{\otimes w} = \prod_{s=0}^{w-1} U_s (|0^n\rangle^{\otimes w}) = \left( \frac{1}{\|\mathbf{x}\|} \sum_{i=0}^{2^n-1} x_i |i\rangle \right)^{\otimes w} \quad (16)$$

Here  $U_s$ 's are the same quantum state preparation unitary but acting on different  $|0^n\rangle$  states. Even though  $U_s$ 's act on different  $|0\rangle$  states in the data qubit, they can share many of the same ancilla qubits.

We can also prepare many copies of different unentangled quantum states

$$\bigotimes_{d=0}^{w-1} |\psi_j\rangle = \prod_{d=0}^{w-1} U_d (|0^n\rangle^{\otimes w}) = \bigotimes_{d=0}^{w-1} \left( \frac{1}{\|\mathbf{x}^d\|} \sum_{i=0}^{2^n-1} x_i^d |i\rangle \right) \quad (17)$$

Here  $U_d$ 's are *different* quantum state preparation unitaries acting on different  $|0^n\rangle$  states and preparing different  $N$ -dimensional states described by the vector of coefficients  $\mathbf{x}^d$ . Even though each  $U_d$  is mathematically different, the exact quantum gate scheduling is the same. The only difference is the single-qubit rotation angles.

### A. SP + CSP Multi-Copy

In order to prepare the joint state in Eq. (17), we can now let  $U_d = U_{d(\text{CSP})}U_{d(\text{SP})}$ . We first execute all the  $U_{d(\text{SP})}$  circuits in parallel and let  $m = n - \log_2(n)$ . That is, we first perform the operation

$$\prod_{d=0}^{w-1} U_{d(\text{SP})} \left( |0^n\rangle^{\otimes w} \right) = \bigotimes_{d=0}^{w-1} (|\phi_d\rangle \otimes |0^{n-m}\rangle), \quad (18)$$

where  $|\phi_d\rangle$  is defined from  $\mathbf{x}^d$  as in Eq. (5). Then, we jointly execute all the  $U_{d(\text{CSP})}$  circuits.

$$\prod_{d=0}^{w-1} U_{d(\text{CSP})} \left( \bigotimes_{d=0}^{w-1} (|\phi_d\rangle \otimes |0^{n-m}\rangle) \right) = \bigotimes_{d=0}^{w-1} |\psi_d\rangle \quad (19)$$

We do not have sufficient ancillae to perform these circuits in parallel, so we perform them with some “indentation”  $k$  between each other. That is, we begin the  $d = 0$  protocol at layer 0, the  $d = 1$  protocol at layer  $k$ , the  $d = 2$  protocol at layer  $2k$ , etc.

We illustrate the above operation as a quantum circuit in Fig. 9. If we choose  $m = n - \log_2(n)$  The first operation

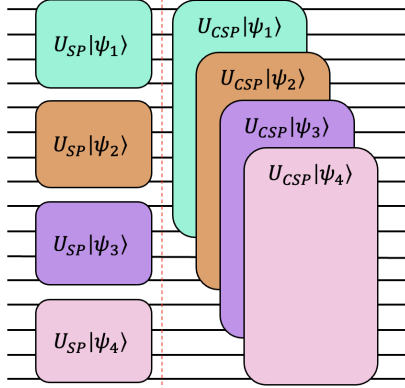


Figure 9: Illustration of stacking different SP + CSP circuit together ( $w = 4$ )

described in Eq. (18) can be achieved in  $O(\log(N))$  depth and  $O(N)$  spacetime allocation. Since each of the  $U_{d(\text{SP})}$  is using  $\frac{N}{\log N}$  qubits, up to  $O(\log N)$  joint states can be parallelized in this way without introducing additional ancilla qubits.

Now let's walk through the second operation described in Eq. (19). The most ancilla-consuming process are the LOADF operations, and in particular, the layer of

doubly-controlled rotation ( $\text{CCR}_y$ ) operations that appear in Fig. 20 of the appendix, which requires  $O(N)$  ancillae in the  $A$  register. Note that these ancillae can be quickly freed up after the parallelized  $\text{CCR}_y$  operations by the CopySwap operation under  $O(N)$  spacetime allocation, as shown in Fig. 20. Thus we can indent the  $U_{\text{CSP}}$  part of the later  $U_d$ 's by some constant number of layers  $k$ .

Besides the  $A$  register that uses  $O(N)$  ancillae, we also have the  $C$ ,  $B$ , and  $F$  registers (as shown in Fig. 20) in the  $U_{\text{CSP}}$  operation. By choosing  $m = n - \log_2(n)$ , we would have negligible ancilla counts for the  $C$  register ( $m \cdot \frac{N}{M} = m \log(N)$  ancillae), the  $B$  register ( $M = \frac{N}{\log(N)}$  ancillae), and the  $F$  register ( $\frac{N}{M} = n$  ancillae). Therefore, they won't contribute much to the overall spacetime allocation cost.

We offer a toy model gate-level illustration in Fig. 10. We can see that the circuit depth will be  $2w + \log N$  instead of  $w \log N$ . The number of ancillae used is upper bounded by  $8N$ .

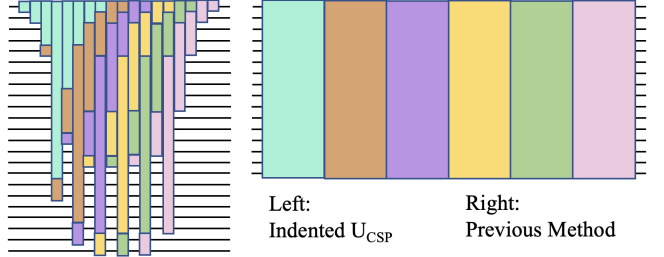


Figure 10: Illustration of stacking a portion of the  $U_{\text{CSP}}$  circuit (LOADF) with indentation  $k = 2$ .

When using the  $\{\text{H}, \text{S}, \text{T}, \text{CNOT}\}$  gate set, one can develop specific compilation strategies that utilize this early-ancilla-free-up structure based on the particular  $\epsilon$  values.

## V. APPLICATIONS

In general, quantum measurements are probabilistic. Therefore, for many quantum algorithms, we typically need to run many shots with the same quantum circuit setup. That is, we will need to execute the entire circuit (state preparation, algorithm circuit, and measurement) many times to get enough measurement precision. Therefore, for many quantum algorithms that require multiple shots/executions and arbitrary quantum state preparation, our novel state preparation method would have at least a constant advantage.

However, there exist even stronger cases where our novel encoding methods can provide advantages regardless of the measurement precision, including but not limited to: quantum machine learning, Hamiltonian simulation, and solving linear systems with algorithms in

the style of the Harrow-Hassidim-Lloyd (HHL) algorithm [13].

### A. Quantum Machine Learning

#### 1. Batching

One of the proposed quantum advantages for machine learning tasks is utilizing quantum computers' exponential Hilbert space to encode and process data, potentially providing super-polynomial speedup over classical machine learning methods. One of the bottlenecks to realizing such an advantage is that encoding the classical data onto the quantum machine in the exponential compact form (*amplitude encoding*) is costly. In amplitude encoding, we wish to encode the feature vector  $\mathbf{x} = [x_0, x_1, \dots, x_{N-1}]$  into the amplitude of the quantum state such that

$$|\psi\rangle = \frac{1}{\|\mathbf{x}\|} \sum_{i=0}^{N-1} x_i |i\rangle \quad (20)$$

Notice that  $N = 2^n$ , where  $n$  is the number of required qubits. This indicates we can encode the feature vector in an exponentially compact way.

For instance, if we have a  $2 \times 2$  image that has a pixel value array of [232, 31, 62, 137] (each pixel can have color values ranging from 0 - 255), the corresponding encoded state would be:

$$|\psi\rangle = 0.834|00\rangle + 0.111|01\rangle + 0.223|10\rangle + 0.492|11\rangle \quad (21)$$

In typical machine learning tasks, we would need to feed many copies of training data into the machine learning models and adjust the parameters in the models with respect to the defined objective values based on each iteration of the training data. One could naively execute these iterations one after another. In the quantum computing setting, one such iteration would involve:

1. encoding one data point into a quantum state via state preparation
2. processing the state with, e.g., a quantum neural network circuit
3. measuring the output and obtaining a single objective value

We would then repeat the above steps until the last training data point, as shown in Fig. 11.

One could also do the batching method, which is to compute several objectives for several data points **simultaneously** and then update the parameters based on some joint properties of the objects (e.g., average), instead of updating the parameters one at a time based on each objective. Now the iteration becomes the following (also depicted in Fig. 12):

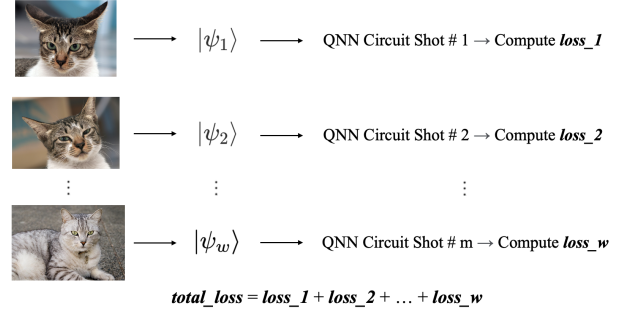


Figure 11: Many-shot method

1. encoding many data points into separate quantum states simultaneously
2. processing all states with, e.g., quantum neural network circuits simultaneously
3. measuring the output of each circuit simultaneously and computing the total loss

With the previous encoding strategy, batching would not bring any differences in the quantum circuit executions except for the parameter updating part. This is because one would either need to multiply the required number of qubits and parallel everything together (Fig. 12) or run many shots to finish each data point separately (Fig. 11), thus offering no difference in the total quantum resource.

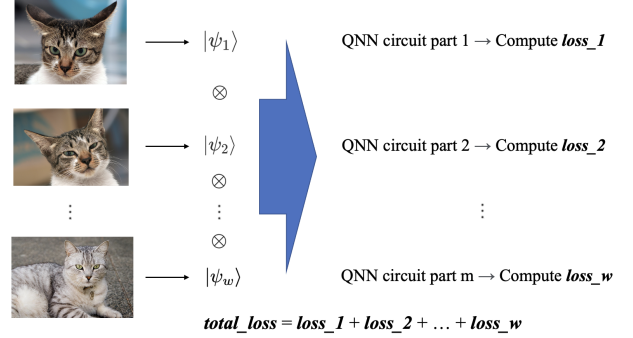


Figure 12: 1-shot method

However, using our SP + CSP encoding method, we could do the 1-shot method with reduced quantum resource requirements. As illustrated in Table III, the required gate depth is reduced asymptotically, from  $O(w \log N)$  to  $O(w + \log N)$ , with only constant-factor additional ancilla introduced.

#### 2. Quanvolutional Neural Network

Henderson et al. [29] has proposed a hybrid quantum-enhanced machine learning method, which is to add

	# Qubits	# Shots	Depth
Depth Efficient	$O(wN)$	1	$O(\log N)$
Qubit Efficient	$O(N + w \log N)$	1	$O(w \log N)$
Multi-Shot	$O(N + w \log N)$	$w$	$O(\log N)$
<b>This Work</b>	<b><math>O(N + w \log N)</math></b>	<b>1</b>	<b><math>O(w + \log N)</math></b>

Table III: Amplitude Encoding Resource Comparison Across Various Methods

“quantum” convolution layer(s) before or after the classical convolution layers, as shown in Fig. 13.

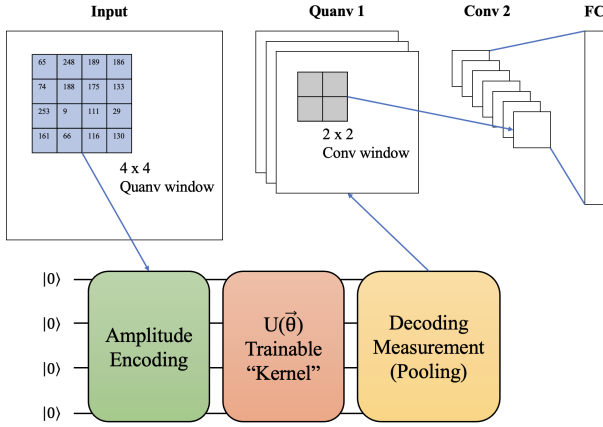


Figure 13: Quanvolutional Neural Network Example: the input data is first encoded into the amplitude form, combined with a trainable “kernel” and a decoder to form a quanvolutional layer (Quanv 1). Then the resulting quanvolutional layer is further passed down to another classical convolutional layer (Conv 2), followed by a fully connected layer (FC).

The general idea is to first encode the classical input data (whether it is directly from the image input or from a previous classical layer), then do a variational circuit (so that this “quantum filter” is now trainable), and then pass down the quantum circuit measurement result to the later classical layer. To put in the machine learning language, this process would correspond to inserting a convolution layer with  $l \times l$  sized kernels, where each kernel can be encoded as  $\sum_{i=0}^{l^2-1} x_i |i\rangle$  quantum states if using the amplitude encoding with proper padding.

In Henderson et al.’s original proposal, the kernel sizes are small (i.e.,  $2 \times 2$ ). It is true that for many CNN applications using stacked small filters is more efficient than a large kernel, given the same classical computational complexity [30, 31]. However, this might not necessarily be the case for quantum-typed convolutional neural networks, given that higher quantum dimensionality would potentially offer better quantum parallelization. Furthermore, applications like semantic segmentation [32] and receptive field building [33] would naturally favor large kernels even in the classical setting.

Since the kernels need to cover the entire image (or

other learning targets), we would need to run the encoding circuit with different encoding values many times. The “quantum” kernel size and stride (distance between each convolved window) size can be the hyperparameters in the overall training process. Our novel encoding method would have practical advantages once the kernel size and the number of kernels get big.

## B. Hamiltonian Simulation - LCU

Hamiltonian simulation is the task of synthesizing the time evolution unitary  $e^{iHt}$  given a length of time  $t$  and a description of some Hamiltonian  $H$ . One method to perform Hamiltonian simulation is to use linear combination of unitaries (LCU) [9, 38]. Typically, we can approximate the Hamiltonian evolution operator as the Taylor expanded form, truncated to order  $K$ :

$$U(t) = \sum_{k=0}^K \frac{(-itH)^k}{k!} \quad (22)$$

$$= \sum_{j=0}^{\Gamma} \beta_j V_j \quad (23)$$

where  $\Gamma = \sum_{k=0}^K L^k$  ( $L$  is the number of Pauli terms in the Hamiltonian).

To achieve the  $U(t)$  operator on the Hamiltonian data qubit, we can construct the following isometry  $\mathcal{V}$  (a non-invertible operator acting on the Hamiltonian data qubits and some additional ancilla qubits):

$$\mathcal{V}(t) = -WRW^\dagger RW(|0\rangle \otimes I) \quad (24)$$

Where  $R$  is the reflection operation defined as  $R = (I - 2|0\rangle \langle 0|) \otimes I$ , and  $W$  is defined as:

$$W = (B^\dagger \otimes I) \left( \sum_{j=0}^{\Gamma-1} |j\rangle \langle j| \otimes V_j \right) (B \otimes I) \quad (25)$$

Here  $B$  is defined as:

$$B |0\rangle^{\otimes \log \Gamma} = \frac{1}{\sqrt{s}} \sum_{j=0}^{\Gamma-1} \sqrt{\beta_j} |j\rangle \quad (26)$$

Thus, the oracle  $B$  is exactly our quantum state preparation oracle.

In a typical quantum chemistry simulation setting, people generally considered up to two-electron and sometimes three-electron integrals in the second quantized Hamiltonian, which would make  $\Gamma$  go to  $O(n^4)$  [39] and sometimes  $O(n^6)$  [40, 41] in scale (here  $n$  indicates the number of orbitals).

Recent works [34, 42, 43] have shown the advantage of performing **joint measurements** on the end states of the Hamiltonian simulation over separate measurements. That is, we run many instances of the LCU algorithm

	Single Measurement LB	Single Measurement UB	Joint Measurement UB
<b>Shadow Tomography (General)</b>	$\tilde{\Omega}(\min(M, 2^n)/\varepsilon^2)$ [34]	$\tilde{O}(\min(M, 2^n)/\varepsilon^2)$ [35]	$O(n \log^2 M/\varepsilon^2)$ [36]
<b>Shadow Tomography (Pauli)</b>	$\Omega(2^n/\varepsilon^2)$ [34]	$O(n2^n/\varepsilon^2)$ [35]	$O(n/\varepsilon^2)$ [37]

Table IV: Joint measurement vs. single measurement sample complexity lower bounds (LB) and upper bounds (UB) for general shadow tomography and shadow tomography with Pauli observables.  $M$  denotes the number of measurements, and  $n$  denotes the number of qubits for the quantum state we want to measure. The tilde sign  $\sim$  means up to logarithmic factors. Note that here the  $\varepsilon$  indicates the measurement inaccuracy caused by statistical fluctuation, which is distinct from the state precision error  $\epsilon$  defined in the previous sections.

many times, and measure the end state jointly. Doing this would give us a better sample complexity scaling, which in the end, will result in better total circuit complexity by saving the total number of circuit execution in order to reach certain measurement thresholds. This would give another natural advantage for us to simultaneously perform the quantum state preparation oracle inside the LCU algorithm, on top of the  $O(\log(N))$  factors of speedup. We summarize the total circuit resource estimation between different measurement/execution strategies in Table IV, which shows the potential advantage of using shadow tomography.

### C. HHL - Repeat until Success

The classical linear system problem is defined as follows: given an  $N \times N$  matrix  $A$ , and a  $N \times 1$  vector  $\vec{b}$ , find the solution vector  $\vec{x}$  such that  $A\vec{x} = \vec{b}$ . To translate to the quantum setting, we would seek some value related to the solution state  $|x\rangle$  (e.g., some observable  $\langle x| M |x\rangle$ ) such that  $A|x\rangle = |b\rangle$ . Preparing the state  $|b\rangle = \sum a_i |i\rangle$  where  $\vec{b} = [a_1, a_2, \dots, a_N]^T$  is exactly a QSP problem.

If the linear system  $A$  is sparse, classically solving the linear system problem by inverting  $A$  has overall runtime  $O(\kappa N)$  [44], where  $\kappa$  is the condition number of the matrix  $A$ , i.e., the ratio between the largest and the smallest singular value of  $A$ . (Here we ignore complexity dependence on approximation error.) The HHL algorithm [13] was the first quantum algorithm to provide a solution to the quantum linear system problem and runs in depth  $O(\kappa^2 \text{polylog} N)$  overall runtime (subsequent improvement up to  $O(\kappa \text{polylog} N)$  by Costa et al. [45]). The overall runtime  $O(\kappa^2 \text{polylog} N)$  comes from the fact that we need to **repeat** the  $O(\kappa \cdot \text{polylog} N)$  circuit  $O(\kappa)$  times to make sure we land in the correct state  $|1\rangle$  postselecting on the state:

$$\sum_i c_i |v_i\rangle |\lambda_i\rangle \left( \frac{1}{\kappa \lambda_i} |1\rangle + \sqrt{1 - \frac{1}{\kappa^2 \lambda_i^2}} |0\rangle \right) \quad (27)$$

so that the state is then  $\sum_i \frac{c_i}{\lambda_i} |v_i\rangle |\lambda_i\rangle$ , which can be turned into an approximation of  $|x\rangle$  by running eigenvalue estimation in reverse and uncomputing  $\lambda_i$  [14].

In many problems of interest, the state  $|b\rangle$  is not sparse, and the value  $\kappa$  can become very large. These two conditions make our novel encoding method a perfect tool to apply in this setting. Here we can simultaneously prepare  $\kappa$  copies of the same  $|b\rangle$  state more efficiently.

Besides sparse matrices, HHL can also provide speedup for dense matrices. Classically inverting a dense matrix via Gaussian elimination would result in  $O(N^3)$  overall runtime. Using an adapted version of HHL, we can achieve  $O(\kappa^2 \sqrt{N} \text{polylog}(N))$  [15] (including repeating the circuit  $\kappa$  times with phase estimation).

Using our method to execute many HHL iterations together simultaneously, we can get up to  $O(\min(\kappa, \log N))$  factors of speedup versus the original versions. One may also utilize the joint measurement technique to achieve sample complexity advantage for certain HHL problems [34, 42, 43].

Recent work [45, 46] has also proposed the adiabatic version of HHL, which does not require the repeat-until-success process. This will make the overall complexity at  $O(\kappa \sqrt{N} \text{polylog}(N))$  for dense systems. We want to note that the adiabatic version does have large constants, which would make a longer circuit. Effectively this would be a tradeoff between short-and-repeat versus long-and-no-repeat for the algorithm users to choose.

Furthermore, one may utilize the exponential compactness of the amplitude encoding to achieve up to exponential advantage in the communication complexity setting [47].

## VI. ACKNOWLEDGMENT

We thank Connor Hann, Yunong Shi, Erhan Bas, Pei Zeng, Ming Yuan, Siteng Kang, Kyle Brubaker, Martin Schuettz, Fei Chen, Liang Jiang, Eric Kessler, Senrui Chen, and Sisi Zhou for their helpful discussions. This work is funded in part by EPiQC, an NSF Expedition in Computing, under award CCF-1730449. FTC is Chief Scientist for Quantum Software at Infleqtion and an advisor to Quantum Circuits, Inc.

---

[1] J. Biamonte, P. Wittek, N. Pancotti, P. Rebentrost, N. Wiebe, and S. Lloyd, Quantum machine learning, *Nature* **549**, 195 (2017).

[2] S. Lloyd, M. Mohseni, and P. Rebentrost, Quantum principal component analysis, *Nature Physics* **10**, 631 (2014).

[3] I. Kerenidis and A. Prakash, Quantum Recommendation Systems, in *8th Innovations in Theoretical Computer Science Conference (ITCS 2017)*, Leibniz International Proceedings in Informatics (LIPIcs), Vol. 67 (2017) pp. 49:1–49:21.

[4] P. Rebentrost, A. Steffens, I. Marvian, and S. Lloyd, Quantum singular-value decomposition of nonsparse low-rank matrices, *Physical review A* **97**, 012327 (2018).

[5] I. Kerenidis, J. Landman, A. Luongo, and A. Prakash, q-means: A quantum algorithm for unsupervised machine learning, *Advances in Neural Information Processing Systems* **32** (2019).

[6] I. Kerenidis and J. Landman, Quantum spectral clustering, *Physical Review A* **103**, 042415 (2021).

[7] P. Rebentrost, M. Mohseni, and S. Lloyd, Quantum support vector machine for big data classification, *Physical review letters* **113**, 130503 (2014).

[8] M. Schuld and F. Petruccione, *Machine learning with quantum computers* (Springer, 2021).

[9] D. W. Berry, A. M. Childs, R. Cleve, R. Kothari, and R. D. Somma, Simulating Hamiltonian dynamics with a truncated Taylor series, *Physical review letters* **114**, 090502 (2015).

[10] D. W. Berry, A. M. Childs, and R. Kothari, Hamiltonian simulation with nearly optimal dependence on all parameters, in *2015 IEEE 56th annual symposium on foundations of computer science* (IEEE, 2015) pp. 792–809.

[11] G. H. Low and I. L. Chuang, Optimal Hamiltonian simulation by quantum signal processing, *Physical review letters* **118**, 010501 (2017).

[12] G. H. Low and I. L. Chuang, Hamiltonian simulation by qubitization, *Quantum* **3**, 163 (2019).

[13] A. W. Harrow, A. Hassidim, and S. Lloyd, Quantum algorithm for linear systems of equations, *Physical review letters* **103**, 150502 (2009).

[14] A. Ambainis, Variable time amplitude amplification and quantum algorithms for linear algebra problems, in *STACS'12 (29th Symposium on Theoretical Aspects of Computer Science)*, Vol. 14 (LIPIcs, 2012) pp. 636–647.

[15] L. Wossnig, Z. Zhao, and A. Prakash, Quantum linear system algorithm for dense matrices, *Physical review letters* **120**, 050502 (2018).

[16] G. H. Low, V. Kliuchnikov, and L. Schaeffer, Trading T-gates for dirty qubits in state preparation and unitary synthesis, *arXiv preprint arXiv:1812.00954* (2018).

[17] X. Sun, G. Tian, S. Yang, P. Yuan, and S. Zhang, Asymptotically optimal circuit depth for quantum state preparation and general unitary synthesis, *IEEE Transactions on Computer-Aided Design of Integrated Circuits and Systems* (2023).

[18] P. Yuan and S. Zhang, Optimal QRAM and improved unitary synthesis by quantum circuits with any number of ancillary qubits, *arXiv preprint arXiv:2202.11302* (2022).

[19] X.-M. Zhang, T. Li, and X. Yuan, Quantum state preparation with optimal circuit depth: Implementations and applications, *Physical Review Letters* **129**, 230504 (2022).

[20] B. D. Clader, A. M. Dalzell, N. Stamatopoulos, G. Salton, M. Berta, and W. J. Zeng, Quantum resources required to block-encode a matrix of classical data, *IEEE Transactions on Quantum Engineering* (2023).

[21] N. J. Ross and P. Selinger, Optimal ancilla-free Clifford+T approximation of z-rotations., *Quantum Inf. Comput.* **16**, 901 (2016).

[22] R. Babbush, C. Gidney, D. W. Berry, N. Wiebe, J. McClean, A. Paler, A. Fowler, and H. Neven, Encoding electronic spectra in quantum circuits with linear T complexity, *Physical Review X* **8**, 041015 (2018).

[23] I. F. Araujo, D. K. Park, F. Petruccione, and A. J. da Silva, A divide-and-conquer algorithm for quantum state preparation, *Scientific reports* **11**, 1 (2021).

[24] V. V. Shende and I. L. Markov, On the CNOT-cost of Toffoli gates, *arXiv preprint arXiv:0803.2316* (2008).

[25] J. A. Smolin and D. P. DiVincenzo, Five two-bit quantum gates are sufficient to implement the quantum Fredkin gate, *Physical Review A* **53**, 2855 (1996).

[26] Y. Ding, X.-C. Wu, A. Holmes, A. Wiseth, D. Franklin, M. Martonosi, and F. T. Chong, Square: Strategic quantum ancilla reuse for modular quantum programs via cost-effective uncomputation, in *2020 ACM/IEEE 47th Annual International Symposium on Computer Architecture (ISCA)* (IEEE, 2020) pp. 570–583.

[27] M. Plesch and i. c. v. Brukner, Quantum-state preparation with universal gate decompositions, *Phys. Rev. A* **83**, 032302 (2011).

[28] M. A. Nielsen and I. Chuang, Quantum computation and quantum information (2002).

[29] M. Henderson, S. Shakya, S. Pradhan, and T. Cook, Quanvolutional neural networks: powering image recognition with quantum circuits, *Quantum Machine Intelligence* **2**, 1 (2020).

[30] C. Szegedy, W. Liu, Y. Jia, P. Sermanet, S. Reed, D. Anguelov, D. Erhan, V. Vanhoucke, and A. Rabinovich, Going deeper with convolutions, in *Proceedings of the IEEE conference on computer vision and pattern recognition* (2015) pp. 1–9.

[31] K. He, X. Zhang, S. Ren, and J. Sun, Deep residual learning for image recognition, in *Proceedings of the IEEE conference on computer vision and pattern recognition* (2016) pp. 770–778.

[32] C. Peng, X. Zhang, G. Yu, G. Luo, and J. Sun, Large kernel matters—improve semantic segmentation by global convolutional network, in *Proceedings of the IEEE conference on computer vision and pattern recognition* (2017) pp. 4353–4361.

[33] X. Ding, X. Zhang, J. Han, and G. Ding, Scaling up your kernels to 31x31: Revisiting large kernel design in CNNs, in *Proceedings of the IEEE/CVF Conference on Computer Vision and Pattern Recognition* (2022) pp. 11963–11975.

[34] S. Chen, J. Cotler, H.-Y. Huang, and J. Li, Exponential separations between learning with and without quantum memory, in *2021 IEEE 62nd Annual Symposium on Foundations of Computer Science (FOCS)* (IEEE, 2022) pp. 574–585.

- [35] H.-Y. Huang, R. Kueng, and J. Preskill, Predicting many properties of a quantum system from very few measurements, *Nature Physics* **16**, 1050 (2020).
- [36] C. Bădescu and R. O'Donnell, Improved quantum data analysis, in *Proceedings of the 53rd Annual ACM SIGACT Symposium on Theory of Computing* (2021) pp. 1398–1411.
- [37] H.-Y. Huang, R. Kueng, and J. Preskill, Information-theoretic bounds on quantum advantage in machine learning, *Physical Review Letters* **126**, 190505 (2021).
- [38] A. M. Childs, D. Maslov, Y. Nam, N. J. Ross, and Y. Su, Toward the first quantum simulation with quantum speedup, *Proceedings of the National Academy of Sciences* **115**, 9456 (2018).
- [39] T. Helgaker, P. Jorgensen, and J. Olsen, *Molecular electronic-structure theory* (John Wiley & Sons, 2013).
- [40] M. Motta, T. P. Gujarati, J. E. Rice, A. Kumar, C. Masterton, J. A. Latone, E. Lee, E. F. Valeev, and T. Y. Takeshita, Quantum simulation of electronic structure with a transcorrelated Hamiltonian: improved accuracy with a smaller footprint on the quantum computer, *Physical Chemistry Chemical Physics* **22**, 24270 (2020).
- [41] S. McArdle and D. P. Tew, Improving the accuracy of quantum computational chemistry using the transcorrelated method, arXiv preprint arXiv:2006.11181 (2020).
- [42] S. Bubeck, S. Chen, and J. Li, Entanglement is necessary for optimal quantum property testing, in *2020 IEEE 61st Annual Symposium on Foundations of Computer Science (FOCS)* (IEEE, 2020) pp. 692–703.
- [43] H.-Y. Huang, M. Broughton, J. Cotler, S. Chen, J. Li, M. Mohseni, H. Neven, R. Babbush, R. Kueng, J. Preskill, *et al.*, Quantum advantage in learning from experiments, *Science* **376**, 1182 (2022).
- [44] J. R. Shewchuk *et al.*, An introduction to the conjugate gradient method without the agonizing pain (1994).
- [45] P. C. Costa, D. An, Y. R. Sanders, Y. Su, R. Babbush, and D. W. Berry, Optimal scaling quantum linear-systems solver via discrete adiabatic theorem, *PRX Quantum* **3**, 040303 (2022).
- [46] Y. Subaşı, R. D. Somma, and D. Orsucci, Quantum algorithms for systems of linear equations inspired by adiabatic quantum computing, *Phys. Rev. Lett.* **122**, 060504 (2019).
- [47] A. Montanaro and C. Shao, Quantum communication complexity of linear regression, arXiv preprint arXiv:2210.01601 (2022).

## Appendix A: Circuit implementations

### 1. Qubit Data Copying

Our implementation of SPF and FLAG circuits will require additional ancillae that are used as part of coherent data copying subroutines. That is, we perform the isometry

$$\alpha|0\rangle + \beta|1\rangle \mapsto \alpha|0^c\rangle + \beta|1^c\rangle \quad (\text{A1})$$

using only CNOT gates, and in depth  $\lceil \log_2(c) \rceil$ . We will need this subroutine because we often want to perform many CSWAP gates with disjoint targets but controlled by the same register. We can accomplish this in shallower depth by copying the control register and applying the CSWAPs in parallel. Clader et al. [20] avoided this issue by assuming the ability to do FANOUT-CNOT with an arbitrary number of targets, which is a Clifford gate, in a single time step.

The protocol for copying consists of  $\lceil \log_2(c) \rceil$  sequential depth-1 operations, labeled by  $\oplus_0, \dots, \oplus_{\lceil \log_2(c) \rceil - 1}$ . We refer to these as *copying layers*. In particular,  $\oplus_j$  consists of a single layer of  $2^j$  parallel CNOTs where the targets of the CNOTs are fresh ancillae. This is illustrated in Fig. 14 and described in Algorithm 3. Notably, while the total number of qubits is  $c$  and the depth is  $\lceil \log_2(c) \rceil$ , most of the ancillae need not be allocated until close to the end of the protocol, and thus the spacetime allocation is  $O(c)$ , rather than  $O(c \log(c))$ .

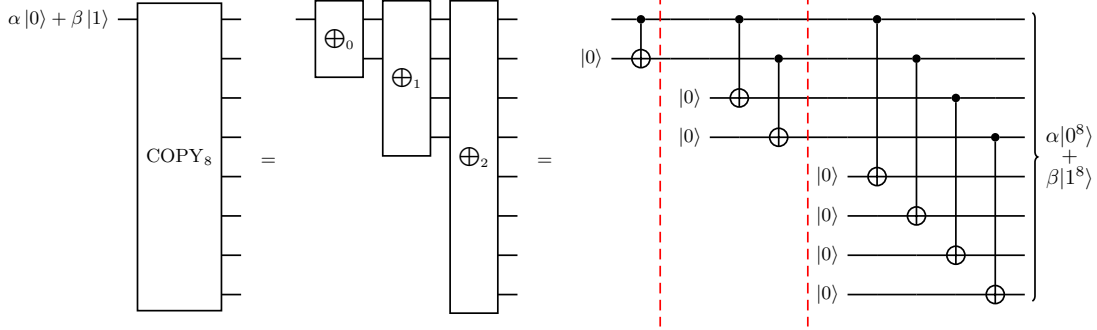


Figure 14: Example circuit implementing state copy subroutine for  $c = 8$  qubits. An arbitrary single-qubit state  $\alpha|0\rangle + \beta|1\rangle$  is copied into  $c = 2^t$  qubits (in the sense of mapping to  $\alpha|0^c\rangle + \beta|1^c\rangle$ ) via a series of  $t$  layers of CNOTs, denoted  $\oplus_0, \dots, \oplus_{t-1}$ . The  $c - 1$  qubits are fresh ancilla qubits that begin in the state  $|0\rangle$ . The depth is  $\log_2(c)$ , and the spacetime allocation is only  $c$ , as seen in the right diagram, by waiting to allocate ancillae until the final moment that they are needed.

---

### Algorithm 3 State-Copy Subroutine

---

```

1: procedure COPYc(R)                                 $\triangleright R$  is a register of size  $c$ , where  $c$  is assumed to be the power of 2 for simplicity
2:   for i in range( $\log_2(c)$ ) do                       $\triangleright$  Each value of  $i$  occupies  $O(1)$  depth
3:      $\oplus_i(R)$ 
4:   end for
5: end procedure
6: procedure  $\oplus_t(R)$                                  $\triangleright$  All values of  $j$  performed in parallel
7:   for j in range( $2^t$ ) do
8:     CNOT( $R_{jc2^{-t}}$ ,  $R_{jc2^{-t}+c2^{-t-1}}$ )
9:   end for
10: end procedure                                      $\triangleright$  Total Dexact:  $\log_2(c)$ 
                                                  $\triangleright$  Total Dapprox:  $\log_2(c)$ 
                                                  $\triangleright$  Total SAexact:  $2c - 2$ 
                                                  $\triangleright$  Total SAapprox:  $2c - 2$ 

```

---

## 2. Parallel CSWAP

With the help of the State-Copy subroutine, we can now effectively perform the parallel CSWAP operations using single-qubit gates and two-qubit CNOT gates, without using the FANOUT-CNOT gate that was required in Ref. [20] to perform the parallel CSWAP when sharing the same control bits.

We denote a layer of  $2^t$  parallel CSWAPs by  $CS_t$ , as depicted in Fig. 15 and algorithm 4.

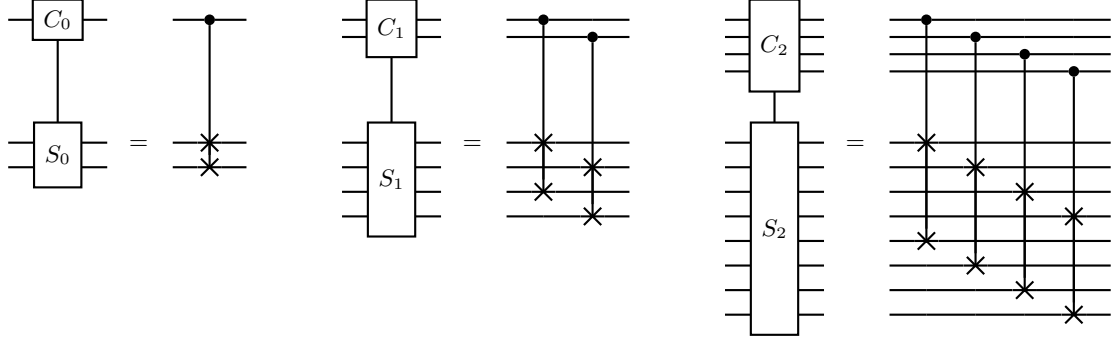


Figure 15: Implementation of  $CS_t$  gate for  $t = 0, 1, 2$ , which can be accomplished in one layer of parallel CSWAP gates.

---

#### Algorithm 4 Parallel CSWAP

---

```

1: procedure  $CS_t(R, S)$ 
    $\triangleright t$ : number of parallel control-swaps,  $R$ : control bit data register with at least  $2^t$  qubits,  $S$ : target bit angle register with at least  $2^{t+1}$  qubits (note that the subscript here labels the qubit indices of every single register)
2:   for  $i$  in range( $2^t$ ) do  $\triangleright$  All values of  $i$  performed in parallel
3:     CSWAP( $R_i, S_i, S_{i+2^t}$ )
4:   end for
5: end procedure

```

---

### 3. SPF

Now we describe the implementation of the SPF gate. The gate acts on  $m + M - 1$  qubits, and our implementation uses additional  $M/2 - m$  ancillae that begin in and end in  $|0\rangle$ . The circuit is similar to that described in Ref. [20], but in our implementation, all gates are two-qubit gates. The idea is to enact  $R_y(\theta_{s,p})$  rotations onto the  $m$  data qubit registers in sequence, but where which pair  $(s, p)$  is used for the  $s$ th rotation depends on the value of the first  $s - 1$  registers. We assume that each of the  $|\theta_{s,p}\rangle$  states has already been prepared. The rotations are enacted by, for each  $s = 0, \dots, m - 1$ , swapping (“injecting”) the correct  $|\theta_{s,p}\rangle$  state with the  $s$ th data qubit. Exactly one  $\theta_{s,p}$  will be injected for each  $s$ . Since  $(0, 0)$  is the only  $(s, p)$  with  $s = 0$ , the first step is to swap  $|\theta_{0,0}\rangle$  with the first data qubit. The second step is to, conditioned on the first data register being  $|1\rangle$ , swap the registers holding  $|\theta_{1,0}\rangle$  and  $|\theta_{1,1}\rangle$ , and then inject the register originally holding  $|\theta_{1,0}\rangle$  into the second data register (using a swap gate). In general, the  $s$ th rotation is enacted by first swapping the correct  $|\theta_{s,p}\rangle$  to the top of the size- $2^s$  register initially holding the states  $|\theta_{s,p}\rangle$ , and then swapping the top register into the  $s$ th data qubit. Naively, this would seem to require at least  $O(m^2)$  depth, as there are  $m$  rotations, and deciding which qubit to inject for each requires  $O(m)$  rounds of controlled-swapping. Ref. [20] observed that this can be reduced to  $O(m)$  depth assuming access to FANOUT-CNOT with  $O(M)$  targets that act in unit time. To decompose such a FANOUT-CNOT gate into two-qubit gates, at least  $O(m)$  depth would typically be required; thus, the depth of the Clader et al. [20] SPF implementation in the  $\{U(2), \text{CNOT}\}$  gate set would be  $O(m^2)$ , not  $O(m)$ .

We give a circuit compilation method for reducing the depth back to  $O(m)$  using a few extra ancillae. We do so by interspersing the CSWAPs with copying layers. In particular, data qubit  $s$  is needed to control  $2^{u-1-s}$  CSWAPs on the angle register that starts in state  $|\Theta_u\rangle$ . Thus, once we have applied  $u - 1 - s$  copying layers to it, we are free to perform the CSWAPs in parallel; we denote the operation that performs  $2^t$  CSWAPs in parallel by  $CS_t$ . While we apply CSWAPs controlled on data qubit  $i$ , we are free to copy other data qubits in parallel. Overall, we manage to perform the operation in only  $O(m)$  depth.

We describe the SPF circuit in several ways. In Fig. 16, we give a complete example of SPF for  $m = 4$ , illustrating how ancilla qubits are used to host copies of the data qubits for the purpose of swapping. However, it is hard to fully see the pattern for small values of  $m$ . In Fig. 17, we show the first half of the SPF gate for a larger  $m = 7$  example and we also label the various registers. In this figure, one can easily verify that the depth is  $O(m)$ . Finally, in algorithm 5, we give pseudocode for the implementation of SPF, consistent with the labels appearing in Fig. 17. To understand the idea behind the circuits, we now describe several rules that must be obeyed (and the reasoning why):

1.  $\bigoplus_j(D_q)$  needs to happen after  $\bigoplus_i(D_q)$  if  $j < i, \forall q$ :
  - This is true by construction, shown in Fig. 14
2.  $\bigoplus_j(D_q)$  needs to happen after  $\text{SWAP}(D_{q,0}, A_{q,0}), \forall j, \forall q$ :
  - This is because the injection of the angle state into data qubit  $q$  must occur before we can begin to copy data qubit  $q$
3.  $CS_k(D_q, \cdot)$  needs to happen after  $\bigoplus_{k-1}(D_q), \forall q$ :
  - This makes sure we can have enough qubits for the CSWAP sequence to control on in order to guarantee maximal parallelization
4.  $CS_j(A_q)$  needs to iterate through all  $j$  values in the order of  $q - 1$  to 0 before  $\text{SWAP}(D_{q,0}, A_{q,0}), \forall q$ :
  - This makes sure all the values are swapped into the correct place for the current qubit based on the previous qubits’ amplitudes before the current qubit is pumped into the data register

Because of the existence of criteria #2 and #4, we cannot simply execute the STATE-COPY subroutine at one time from each  $D_q$  as we do in the FLAG circuit compilation presented in the next subsection (algorithm 6). Doing that would result in  $O(m^2)$  depth. Therefore, we have to intersperse the CSWAP sequences with the copying layers.

The total number of copying layers of data qubits  $j$  that we need is  $m - 2 - j$  (for  $j = 0, \dots, m - 3$ ). Data qubits  $m - 2$  and  $m - 1$  need not be copied. Thus, the total number of ancillae needed is  $\sum_{j=0}^{m-3} (2^{m-2-j} - 1) = 2^{m-1} - m$ .

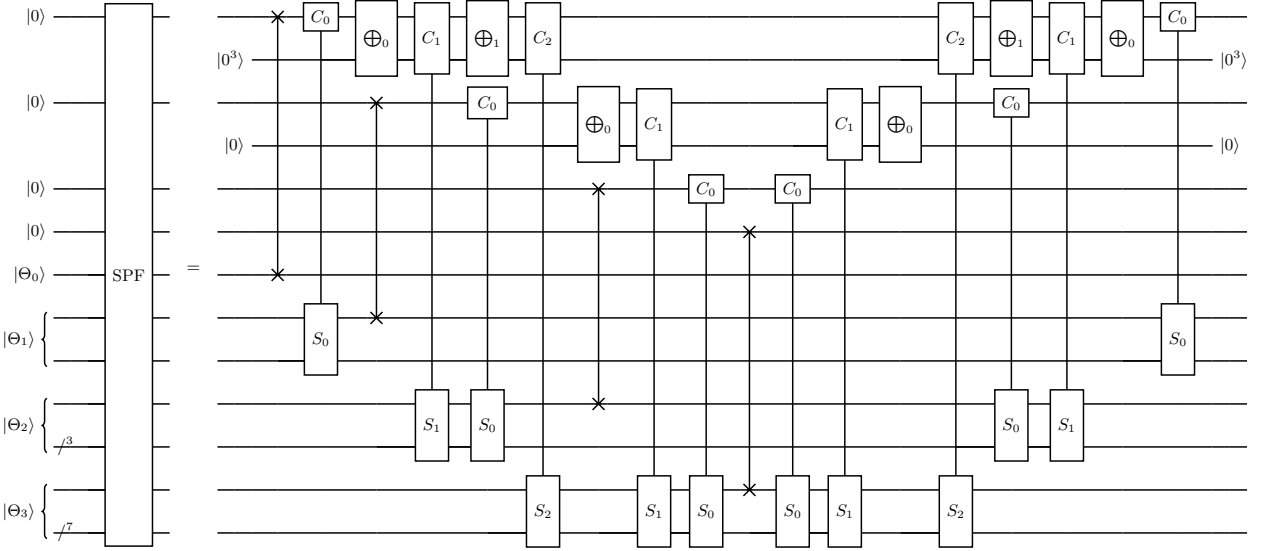


Figure 16: SPF circuit for preparing a state with  $m = 4$  qubits, which are left entangled with  $2^q - 1$  qubits (garbage). The circuit has depth  $O(m)$  and uses an additional  $O(2^m)$  ancillae that begin and end in  $|0\rangle$ . Thus, the total spacetime allocation is upper bounded by  $O(m2^m)$ . The second half of the SPF circuit is very similar to the reverse of the first half except that SWAP gates are not present.

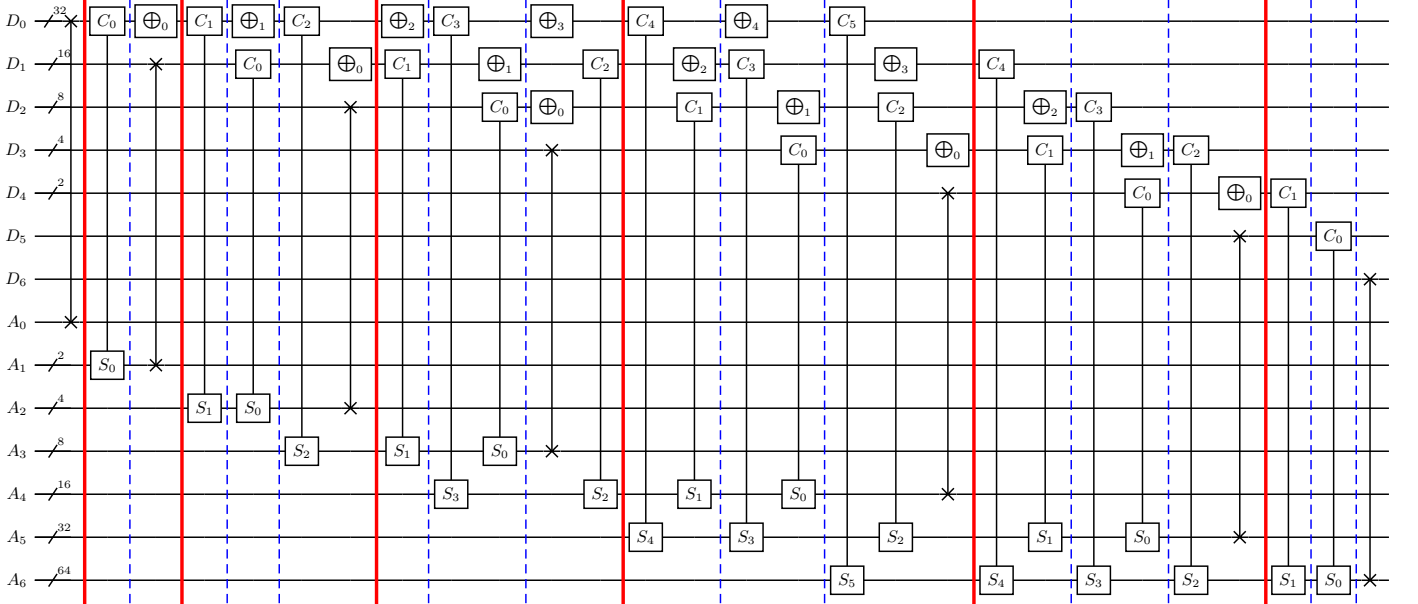


Figure 17: First part of SPF for  $m = 7$ . The circuit consists of 7 data registers ( $D_0 - D_6$ ) and 7 ancilla registers ( $A_0 - A_6$ ). Each space between the red line in the circuit represents 1 iteration of the  $i$  values in algorithm 5. There are 3 parallelized gate sequences in each of the red line spaces, separated by the blue dashed line. The first parallelized gate sequence corresponds to the first for loop in line 3 - line 9. The second parallelized gate sequence corresponds to the second for loop in line 10 - line 16. The third parallelized gate sequence corresponds to the third for loop in line 17 - line 25. (Notice that we might not have all 3 sequences in all of the boxes based on the condition, for instance, at the beginning of the circuit)

**Algorithm 5** SPF Subroutine

---

```

1: procedure SPF( $D, A, m$ ) ▷  $D$  is the data register of size  $m$ 
2:   for  $i$  in range( $m$ ) do ▷  $A = A_0, \dots, A_{m-1}$  is the angle register where  $A_j$  is size  $2^j$ 
3:     for  $q$  in range( $i - 1$ ) do ▷ 1st parallelized sequence in the space between red lines in Fig. 17. All  $q$  in parallel
4:       if  $(i - q)$  is odd and  $\frac{3(i-q-1)}{2} - 1 \leq m - q - 3$  then ▷ Each value of  $i$  occupies  $O(1)$  depth, shown as one box in Fig. 17
5:          $\bigoplus_{\frac{3(i-q-1)}{2}}^{-1}(D_q)$ 
6:       else if  $(i - q)$  is even and  $\frac{3(i-q)}{2} - 2 \leq m - q - 2$  then
7:         CS $_{\frac{3(i-q)}{2}-2}(D_q, A_{i-1+\frac{i-q}{2}})$ 
8:       end if
9:     end for
10:    for  $q$  in range( $i$ ) do ▷ 2nd parallelized sequence in the space between red lines in Fig. 17. All  $q$  in parallel
11:      if  $(i - q)$  is odd and  $\frac{3(i-q-1)}{2} \leq m - q - 2$  then
12:        CS $_{\frac{3(i-q-1)}{2}}(D_q, A_{i+\frac{i-q-1}{2}})$ 
13:      else if  $(i - q)$  is even and  $\frac{3(i-q)}{2} - 2 \leq m - q - 3$  then
14:         $\bigoplus_{\frac{3(i-q)}{2}-2}^{-1}(D_q)$ 
15:      end if
16:    end for
17:    for  $q$  in range( $i + 1$ ) do ▷ 3rd parallelized sequence in the space between red lines in Fig. 17. All  $q$  in parallel
18:      if  $i == q$  then
19:        SWAP( $D_{q,0}, A_{i,0}$ )
20:      else if  $(i - q)$  is odd and  $\frac{3(i-q-1)}{2} \leq m - q - 3$  then
21:         $\bigoplus_{\frac{3(i-q-1)}{2}}^{-1}(D_q)$ 
22:      else if  $(i - q)$  is even and  $\frac{3(i-q)}{2} - 1 \leq m - q - 2$  then
23:        CS $_{\frac{3(i-q)}{2}-1}(D_q, A_{i+\frac{i-q}{2}})$ 
24:      end if
25:    end for
26:  end for
27:  for  $i$  in reversed(range( $1, m$ )) do ▷ Each value of  $i$  occupies  $O(1)$  depth, run in reversed order
28:    for  $q$  in range( $i + 1$ ) do ▷ All values of  $q$  performed in parallel
29:      if  $i == q$  then
30:        continue
31:      else if  $(i - q)$  is odd and  $\frac{3(i-q-1)}{2} \leq m - q - 3$  then
32:         $\bigoplus_{\frac{3(i-q-1)}{2}}^{-1}(D_q)$ 
33:      else if  $(i - q)$  is even and  $\frac{3(i-q)}{2} \leq m - q - 2$  then
34:        CS $_{\frac{3(i-q)}{2}-1}(D_q, A_{i+\frac{i-q}{2}})$ 
35:      end if
36:    end for
37:    for  $q$  in range( $i$ ) do ▷ All values of  $q$  performed in parallel
38:      if  $(i - q)$  is odd and  $\frac{3(i-q-1)}{2} \leq m - q - 2$  then
39:        CS $_{\frac{3(i-q-1)}{2}}(D_q, A_{i+\frac{i-q-1}{2}})$ 
40:      else if  $(i - q)$  is even and  $\frac{3(i-q)}{2} - 2 \leq m - q - 3$  then
41:         $\bigoplus_{\frac{3(i-q)}{2}-2}^{-1}(D_q)$ 
42:      end if
43:    end for
44:    for  $q$  in range( $i - 1$ ) do ▷ All values of  $q$  performed in parallel
45:      if  $(i - q)$  is odd and  $\frac{3(i-q-1)}{2} - 1 \leq m - q - 3$  then
46:         $\bigoplus_{\frac{3(i-q-1)}{2}}^{-1}(D_q)$ 
47:      else if  $(i - q)$  is even and  $\frac{3(i-q)}{2} - 2 \leq m - q - 2$  then
48:        CS $_{\frac{3(i-q)}{2}-2}(D_q, A_{i-1+\frac{i-q}{2}})$ 
49:      end if
50:    end for
51:  end for
52: end procedure ▷ Total Dexact:  $O(m)$   
▷ Total Dapprox:  $O(m)$   
▷ Total SAexact:  $O(m2^m)$   
▷ Total SAapprox:  $O(m2^m)$ 

```

---

#### 4. FLAG

The implementation of the FLAG gate is similar to that of the SPF gate, with a few simplifications. Here, the data qubits are only acting as controls, and there is no injection of angles into the data qubits. Thus, we do not need to alternate between copying layers and CSWAP layers; we can simply perform all the copying at the beginning, then all the CSWAPS, then all the uncopying. The conceptual idea behind the FLAG implementation is that a flag is set in the  $p^{\text{th}}$  flag qubit by first flagging qubit 0 and then swapping qubit 0 into the  $p^{\text{th}}$  position using a sequence of CSWAP layers with different data qubits acting as the control. We give an example of FLAG for  $m = 4$  in Fig. 18 and pseudocode for FLAG in algorithm 6.

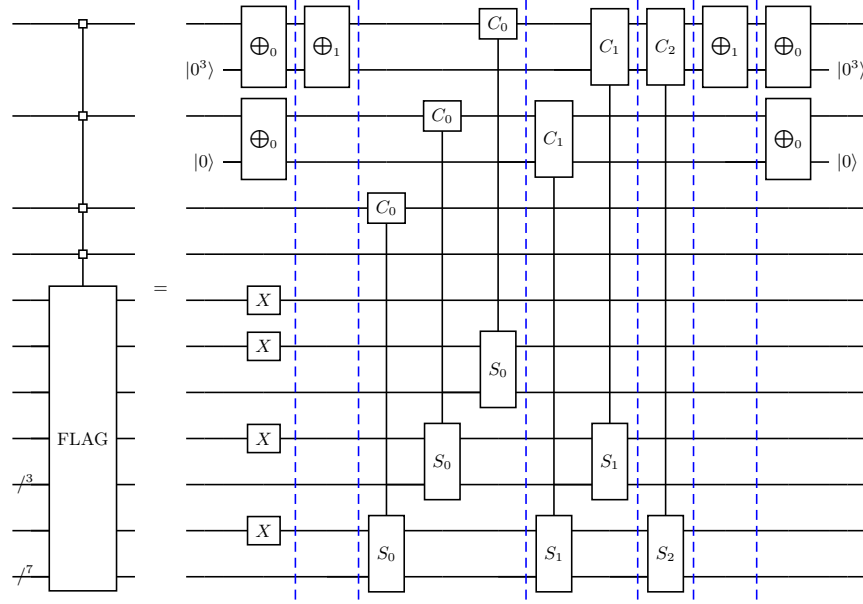


Figure 18: FLAG circuit for  $m = 4$ . All the gate sequences within each of the blue dashed lines can be executed in parallel.

---

**Algorithm 6** FLAG

---

```

1: procedure FLAG SUBROUTINE( $D, F, m$ )
    $\triangleright D = D_0, \dots, D_{m-1}$  is the data register, where  $D_j$  has size  $\max(1, 2^{m-j-2})$ 
    $\triangleright F = F_0, \dots, F_{m-1}$  is the flag register where  $F_j$  has size  $2^j$ 
    $\triangleright$  All values of  $j$  performed in parallel
2:   for  $j$  in range( $m$ ) do
3:      $X(F_{j,0})$ 
4:   end for
5:   for  $i$  in range ( $m - 1$ ) do
6:     COPY( $D_i$ )
7:   end for
8:   for  $i$  in range( $m - 1$ ) do
9:     for  $q$  in range( $m - i - 1$ ) do
10:       $CS_i(D_q, F_{q+1+i})$ 
11:    end for
12:  end for
13:  for  $i$  in range ( $m - 1$ ) do
14:    COPY $^\dagger$ ( $D_i$ )
15:  end for
16: end procedure
    $\triangleright$  Total  $D_{\text{exact}}$ :  $O(m)$ 
    $\triangleright$  Total  $D_{\text{approx}}$ :  $O(m)$ 
    $\triangleright$  Total  $SA_{\text{exact}}$ :  $O(m2^m)$ 
    $\triangleright$  Total  $SA_{\text{approx}}$ :  $O(m2^m)$ 

```

---

## 5. Copy Swap Operation

To simplify the circuit logic of the LOADF subroutines, we define another subroutine operation  $\overline{\text{CopySwap}}$ . To define  $\overline{\text{CopySwap}}$ , let  $|k\rangle$  be an  $m$ -qubit computational basis state, written in binary as  $k_{m-1}k_{m-2}\dots k_0$ , so that  $k_0$  represents the least significant bit. Let  $|\xi\rangle$  be an arbitrary single-qubit state. The operation  $\overline{\text{CopySwap}}$  enacts the isometry from an  $m+1$  qubit state to an  $2M-1$  qubit space

$$\overline{\text{CopySwap}}(|k\rangle|\xi\rangle) = |k_{m-1}\rangle^{\otimes 2^{m-1}}|k_{m-2}\rangle^{\otimes 2^{m-2}}\dots|k_1\rangle^{\otimes 2}|k_0\rangle|0^k\rangle|\xi\rangle|0^{M-k-1}\rangle \quad (\text{A2})$$

for any  $m$ -qubit computational basis state  $|k\rangle$  and any arbitrary single-qubit state  $|\xi\rangle$ . Implementing  $\overline{\text{CopySwap}}$  efficiently will involve a combination of copying layers and layers of parallel CSWAPs, depicted in Fig. 19 using the  $\oplus_t$  and  $\text{CS}_t$  subroutines defined in App. A 1.

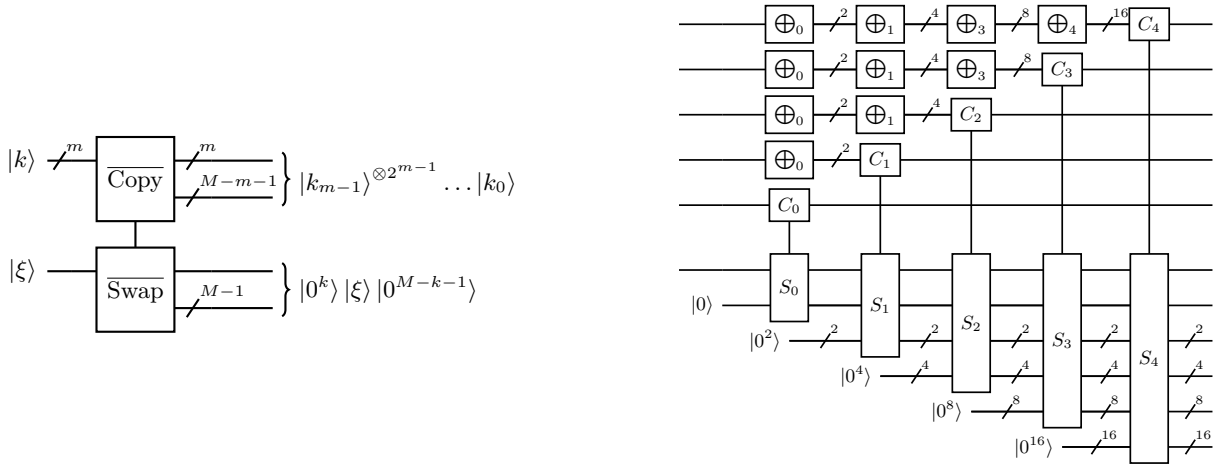


Figure 19: Left: action of  $\overline{\text{CopySwap}}$  operation, which simultaneously copies  $m$  control bits set to  $|k\rangle$  and moves a target register into the  $k$ th position of a target register. The input is  $m+1$  qubits and the output is  $2M-1$  qubits, as several fresh ancillae are introduced during the protocol. Right: implementation of  $\overline{\text{CopySwap}}$  operation using copying layers and swap operations for  $m=5$ . The total depth is  $m$ . At layer  $t=0, \dots, m-1$ , there are

$$(m + (2^t - 1)(m - t) + 2^{t+1}) \text{ active qubits so the total spacetime allocation is}$$

$$\sum_{t=0}^{m-1} (m + (2^t - 1)(m - t) + 2^{t+1}) = O(2^m).$$

## 6. LOADF

The LOADF circuit is perhaps the key to making the whole protocol work. It has two control registers, a data register of size  $m$  and a flag register of size  $D$ . If the data register is set to  $|k\rangle$ , LOADF reads in the  $D$  angle states needed to create the associated  $(n - m)$ -qubit state, but the angle associated with indices  $(s, p)$  is only read in if the flag in position  $(s, p)$  is set to 1.

One key feature of LOADF is that all of the single-qubit rotation gates occur in the same layer of the circuit. This allows it to achieve  $O(\log(N) + \log(1/\epsilon))$  depth in the approximate setting. Another feature is that the  $O(N)$  ancilla qubits are needed only very briefly to act as copied controls for doubly controlled rotation gates. As soon as the rotation gates are finished, the ancilla qubits can be rapidly deallocated, allowing the protocol to achieve  $O(N)$  spacetime allocation. The protocol for LOADF is depicted in Fig. 20.

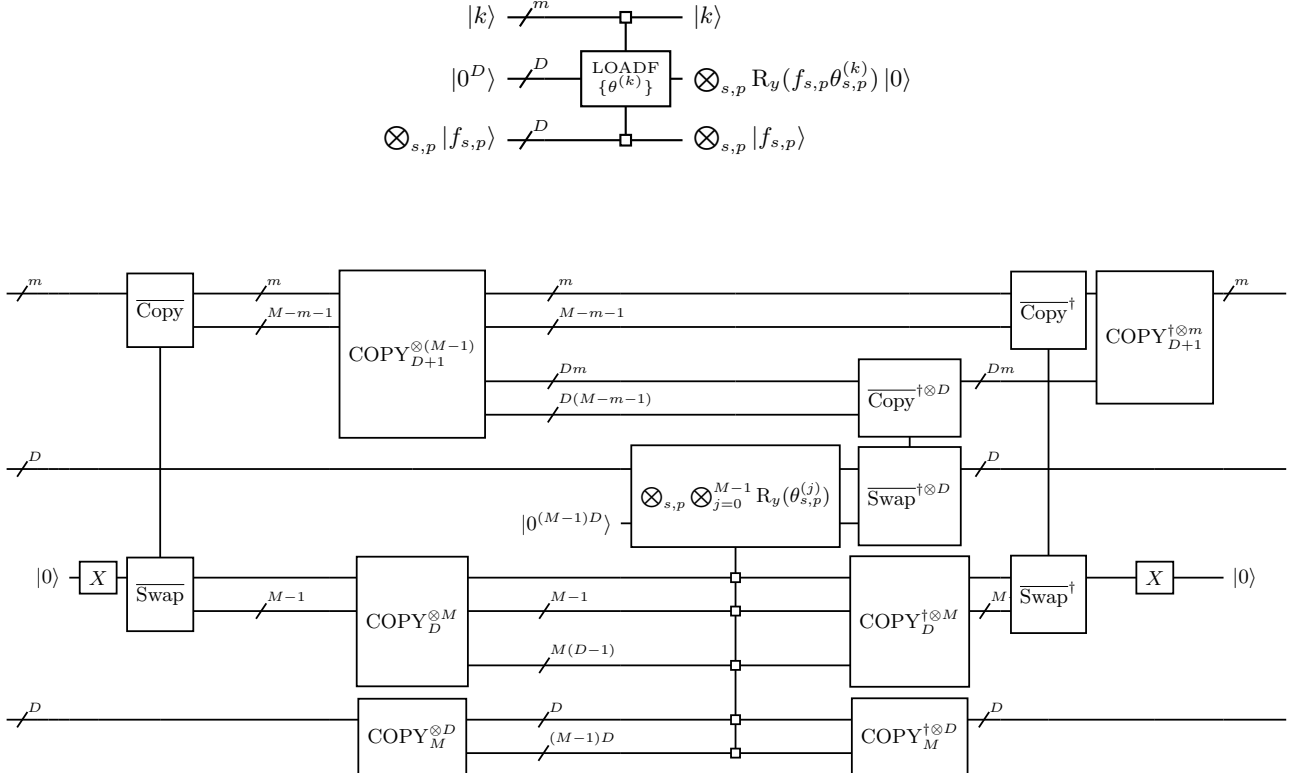


Figure 20: Top: Action of LOADF. Bottom: Circuit implementing LOADF. The parameter  $D$  is defined as  $D := N/M - 1$ . The layer of rotation gates represents  $MD = N - M$  parallel  $CCR_y$  gates by different angles  $\theta_{s,p}^{(k)}$ , with  $k = 0, \dots, M - 1$ ,  $s = 0, \dots, n - m - 1$ , and  $p = 0, \dots, 2^s - 1$ . For each  $CCR_y$  gate, one qubit from the final two registers (corresponding to the choice of  $(s, p)$ ) and one qubit from the three registers above the final two registers (corresponding to the choice of  $k$ ) acts as a control. Copying is necessary such that these can all be performed in parallel. It can be verified that LOADF achieves  $O(N)$  spacetime allocation: the only steps where  $O(N)$  ancillae are active are the rotation gates (depth  $O(1)$ ) and the uncopying step that follows. However, the uncopying step for  $O(N)$  qubits was seen in Figs. 19 and 14 to occupy only  $O(N)$  spacetime allocation.

## Appendix B: Complex amplitudes

The constructions presented in the main text can prepare arbitrary states with real non-negative coefficients. Extending the construction to work for arbitrary coefficients is straightforward. The SP portion of the SP+CSP protocol is unchanged, as the state  $|\phi\rangle$ , as defined in Eq. (5) is insensitive to any phases in the vector  $\mathbf{x}$  (all  $y_i$  are positive). On the other hand, the CSP portion of the protocol must be slightly modified. For each  $k = 0, \dots, M-1$ ,  $j = 0, \dots, N/M-1$ , define the phase

$$e^{i\varphi_j^{(k)}} = \frac{x_{j+kN/M}}{|x_{j+kN/M}|} \quad (\text{B1})$$

(if  $x_{j+kN/M} = 0$ , then the phase can be defined arbitrarily).

Next, we redefine the state  $|\theta_{s,p}^{(k)}\rangle$ :

$$|\theta_{s,p}^{(k)}\rangle = \begin{cases} \cos(\theta_{s,p}^{(k)}/2)|0\rangle + \sin(\theta_{s,p}^{(k)}/2)|1\rangle & \text{if } s < n-m-1 \\ e^{i\varphi_{2p}^{(k)}} \cos(\theta_{s,p}^{(k)}/2)|0\rangle + e^{i\varphi_{2p+1}^{(k)}} \sin(\theta_{s,p}^{(k)}/2)|1\rangle & \text{if } s = n-m-1 \end{cases} \quad (\text{B2})$$

To prepare  $|\theta_{s,p}^{(k)}\rangle$  we need to apply a single-qubit rotation about the  $y$ -axis, and then, if  $s = n-m-1$ , we must apply a single qubit rotation about the  $z$ -axis, as well as a global phase (the global phase will be important when we add controls). To prepare a state with complex amplitudes, the only aspect of the protocol that has to change is the LOADF operation, which appears twice in the circuit for  $U_{\text{CSP}}$  in Fig. 8. As seen in Fig. 20, implementing LOADF involves a doubly controlled  $R_y$  gate. To account for complex amplitudes, we must augment this step with a doubly controlled  $R_z$  gate, and a doubly controlled global phase, which is equivalent to a singly-controlled  $R_z$  gate. These additions lead to at most a constant factor increase in the depth and spacetime allocation. In the approximate  $\{H, S, T, \text{CNOT}\}$  gate set, all rotations need only be synthesized to error  $O(\epsilon/n)$  to achieve overall error  $\epsilon$  in the state preparation protocol, requiring only  $O(\log(n/\epsilon))$  gates per rotation. None of the complexity statements in the paper are impacted.